FACULDADE DE ENGENHARIA DA UNIVERSIDADE DO PORTO

Energy and Performance Aware Multi-Drone Placement for Sustainable Flying Networks

Pedro Miguel Monteiro Ribeiro

Mestrado em Engenharia Eletrotécnica e de Computadores

Supervisor: Professor Rui Lopes Campos

July 28, 2023

Abstract

In recent years, there has been an increasing usage of Unmanned Aerial Vehicles (UAVs) for a wide range of applications. Due to their ability to hover over the ground, they are capable of operating almost everywhere. Additionally, they can carry cargo on-board, which makes them suitable platforms for transporting communications nodes, including Wi-Fi Access Points and cellular Base Stations, giving rise to the concept of Flying Networks (FNs). In scenarios where the deployment of traditional networks is not feasible, the use of FNs emerged to provide wireless connectivity. This is especially relevant in temporary events, such as emergency scenarios and crowded events. However, FNs impose significant challenges regarding the positioning of the UAVs to optimize the Quality of Service (QoS) offered to Ground Users (GUs). Also, contrary to traditional terrestrial network, which are directly connected to the electrical grid, UAVs rely on electrical batteries that need to be recharged. To maximize the UAVs' service time, the energy consumed by the UAVs needs to be minimized. For single UAV placement, some solutions that consider energy consumption have been proposed in the literature. For multi-UAV placement some solutions for UAVs acting as Flying Access Points (FAPs) are available but they are mostly solutions focused on maximizing the coverage area only. However, they do not address the energy-aware multi-UAV placement problem in networking scenarios where the ground users may have different QoS requirements and may not be uniformly distributed across the area.

The main contributions of this dissertation are three-fold: 1) the Sustainable multi-UAV Performance-aware Placement (SUPPLY) algorithm, which defines the energy-aware positioning of multiple UAVs in a Flying Network, while ensuring the target QoS levels; 2) the evaluation of the SUPPLY algorithm for energy-efficiency and network performance perspectives; and 3) the Multi-UAV Energy Consumption (MUAVE) simulator, developed to compute and evaluate the energy consumption of multiple UAVs in an FN.

The evaluation of the SUPPLY algorithm was carried out by means of the MUAVE simulator and the ns-3 simulator. The obtained results show up to 25% energy consumption reduction with minimal impact on average throughput and delay, when compared to keeping the UAVs hovering in the optimal position.

Resumo

Nos últimos anos, tem-se verificado uma utilização crescente de veículos aéreos não tripulados (UAVs) para uma vasta gama de aplicações. Devido à sua capacidade de pairar sobre o solo, eles são capazes de operar praticamente em qualquer lugar. Além disso, podem transportar carga a bordo, o que os torna plataformas adequadas para o transporte de nós de comunicações, incluindo Pontos de Acesso Wi-Fi e Estações Base celulares, dando origem ao conceito de redes voadoras (FNs). Em cenários onde a implementação de redes tradicionais não é viável, a utilização de FNs surge para fornecer conectividade sem fios. Isto é especialmente relevante em eventos temporários, como cenários de emergência e eventos lotados. No entanto, as FNs impõem desafios significativos no que diz respeito ao posicionamento dos UAVs para otimizar a Qualidade de Serviço (QoS) oferecido aos utilizadores terrestres (GUs). Além disso, ao contrário das redes terrestres tradicionais, que estão diretamente ligadas à rede eléctrica, os UAVs dependem de baterias eléctricas que precisam de ser recarregadas. Para maximizar o tempo de serviço dos UAVs, a energia consumida pelos UAVs precisa de ser minimizada. Para o posicionamento de um único UAV, foram propostas na literatura algumas soluções consideram o consumo de energia. Para o posicionamento de múltiplos UAVs, estão disponíveis algumas soluções para UAVs que actuam como Pontos de Acesso Voadores (FAPs), mas a maior parte delas foca-se apenas na maximização da área de cobertura. No entanto, não abordam o problema do posicionamento sensível ao consumo de energia de múltiplos UAVs em cenários de rede em que os utilizadores terrestres podem ter diferentes requisitos de QoS e podem não estar uniformemente distribuídos pela área.

As principais contribuições desta dissertação são três: 1) o algoritmo *Sustainable multi-UAV Performance-aware Placement* (SUPPLY), que define o posicionamento sensível ao consumo de energia de múltiplos UAVs numa rede voadora, garantindo os níveis de QoS alvo; 2) a avaliação do algoritmo SUPPLY do ponto de vista da eficiência energética e do desempenho da rede; e 3) o simulador *Multi-UAV Energy Consumption* (MUAVE), desenvolvido para calcular e avaliar o consumo de energia de múltiplos UAVs numa FN.

A avaliação do algoritmo SUPPLY foi realizada através do simulador MUAVE e do simulador ns-3. Os resultados obtidos mostram uma redução de até 25% no consumo de energia com um impacto mínimo no débito binário e atraso médios, quando comparado a manter os UAVs a pairar na posição óptima.

Acknowledgments

I would like to start by expressing my gratitude and appreciation to my supervisor, Professor Rui Campos, and to my supervisor at INESC TEC, Eng. André Coelho, for their invaluable support and guidance during this dissertation.

I am also grateful to my family for raising me and giving me everything I needed to reach where I am today.

Finally, I am thankful to my friends for their support and for letting me disappear for a while and still be there when I return.

Pedro Ribeiro

Contents

1 Introduction **1**
- 1.1 Motivation and Problem . . . 1
- 1.2 Objectives . . . 2
- 1.3 Contributions . . . 2
- 1.4 Document Structure . . . 3

2 State of the Art **5**
- 2.1 Flying Networks . . . 5
- 2.2 Energy Consumption in Flying Networks . . . 5
  - 2.2.1 UAV Flying Speed . . . 6
  - 2.2.2 UAV Altitude and Payload Weight . . . 6
  - 2.2.3 Energy Consumption Models . . . 7
- 2.3 UAV Placement . . . 10
  - 2.3.1 Single UAV Placement . . . 10
  - 2.3.2 Multi-UAV Placement . . . 14
- 2.4 Summary . . . 18

3 Sustainable multi-UAV Performance-aware Placement Algorithm **19**
- 3.1 Problem Statement . . . 19
- 3.2 System Model and Problem Formulation . . . 19
- 3.3 Sustainable multi-UAV Performance-aware Placement Algorithm . . . 23
- 3.4 Summary . . . 27

4 Multi-UAV Energy Consumption Simulator **29**
- 4.1 Simulator Input Parameters . . . 29
- 4.2 Simulator Implementation . . . 31
- 4.3 Simulator Output . . . 33
- 4.4 Summary . . . 35

5 SUPPLY Evaluation **37**
- 5.1 Energy Consumption and Network Performance Evaluation . . . 37
  - 5.1.1 ns-3 Simulation Setup . . . 38
  - 5.1.2 Evaluation Under Typical Networking Scenarios . . . 38
  - 5.1.3 Energy Evaluation for Random Networking Scenarios . . . 48
- 5.2 Discussion . . . 49

6 Conclusions and Future Work **51**

A **53**

A.1 Additional Multi-UAV Energy Consumption Simulator Outputs 54

A.2 Additional Energy Consumption Results 55

A.3 Additional Network Performance Results 56

References **59**

List of Figures

1.1 Flying Network providing Internet connectivity to the spectators in a music festival [1]. . . . 2

2.1 Propulsion power consumption versus UAV speed for rotary-wing UAV [2]. . . . 6
2.2 Required power to hover over Moscow (124m), Ankara (938 m), and Mexico City (2240 m) as a function of payload weight [3]. . . . 7
2.3 Comparison all models for power consumption [4]. . . . 8
2.4 Comparison of the proposed LSTM model with the ground truth [4]. . . . 9
2.5 Sensitivity of power consumption to key features [4]. . . . 9
2.6 UAV Communication Model [3]. . . . 11
2.7 Optimum height for different QoS requirements, considering γ_{min} equal to 10, 15 and 20 dB, as a function of the power required for hovering [3]. . . . 12
2.8 Simulation scenarios considered in the evaluation of the GWP algorithm [5]. . . . 12
2.9 Intersection of the spheres of two FAPs and candidate FCR trajectories defined by EREP/EPAP [1]. . . . 13
2.10 Flying network organized into a two-tier architecture. An example trajectory defined by EREP/EPAP to minimize the FCR UAV energy consumption is depicted by the red arrows [1]. . . . 13
2.11 NetPlan multi-UAV placement for two scenarios, depicting the AFGs (blue), the FAPs/RFGs (red) and their Wi-Fi cells (green) [6]. . . . 14
2.12 SLICER result for a networking scenario composed of multiple GUs (blue squares) served by two FAPs (green stars). The GUs are associated with two network slices made available in different subareas. [7] . . . 15
2.13 Horizontal Positioning of FAPs [8]. . . . 16
2.14 Multi-UAV Wireless Communications System [9]. . . . 17
2.15 UAV network with the actor–critic algorithm [10]. . . . 17

3.1 Network architecture considered in this dissertation. . . . 20
3.2 MCS index information for the IEEE 802.11ac technology [11]. . . . 21
3.3 Fitting curves of power consumption in circular flight for a rotary-wing UAV [12]. 22
3.4 Example of grouping result for a 10 GUs scenario. The GUs are represented by blue squares and the FAPs by orange triangles. The doted lines indicate wireless links between the nodes. . . . 25
3.5 Intersection area perimeter and SUPPLY trajectories. . . . 26

4.1 Illustrative intersection area. . . . 31
4.2 Representative output for all intersection areas defined by the MUAVE simulator in a 3D representation. Each intersection area is represented by a unique color. . . 33
4.3 Representative output of energy consumption per hour results. . . . 34

4.4 Representative text file with a trajectory description. From left to right, each line indicates the target time, *x* coordinate, and *y* coordinate for each trajectory waypoint. 34

5.1 Comparison of energy consumption per hour for 2 GUs in the same group. 39
5.2 Network performance results for 2 GUS in the same group. 40
5.3 Network performance results, considering the Rician fast-fading component, for 2 GUS in the same group. 40
5.4 Network performance results, considering the Rician fast-fading component and SNR margin of 1 dB, for 2 GUS in the same group. 40
5.5 Comparison of energy consumption per hour for 2 GUs in 2 separate groups. . . 41
5.6 Network performance results for 2 GUS in separate groups. 42
5.7 Comparison of energy consumption per hour for 5 GUs in the same group. 42
5.8 Network performance results for 5 GUS in the same group. 43
5.9 Network performance results, considering the Rician fast-fading component, for 5 GUS in the same group. 43
5.10 Network performance results, considering the Rician fast-fading model and SNR margin of 1 dB, for 5 GUS in the same group. 44
5.11 Comparison of energy consumption per hour for 5 GUs in 2 separate groups. . . 44
5.12 Network performance results for 5 GUS in 2 separate groups. 45
5.13 Comparison of energy consumption per hour for 10 GUs in the same group. . . . 46
5.14 Network performance results for 10 GUS in the same group. 46
5.15 Network performance results, considering the Rician fast-fading component, for 10 GUs in the same group. 46
5.16 Network performance results, considering the Rician fast-fading component and SNR margin of 1 dB, for 10 GUS in the same group. 47
5.17 Comparison of energy consumption per hour for 10 GUs in 2 separate groups. . . 48
5.18 Network performance results for 10 GUS in 2 separate groups. 48
5.19 Energy ratios for the SUPPLY algorithm in relation to the hovering state considering 200 random networking scenarios for each distinct number of GUs – 2, 5, and 10. 49

A.1 Representative terminal output of the Multi-UAV Energy Consumption Simulator. 54
A.2 Comparison of energy consumption per hour for 2 GUs in the same group with a 1 dB SNR margin. 55
A.3 Comparison of energy consumption per hour for 5 GUs in the same group with a 1 dB SNR margin. 55
A.4 Comparison of energy consumption per hour for 10 GUs in the same group with a 1 dB SNR margin. 56
A.5 Network performance results, considering the Rician fast-fading component, for 2 GUS in 2 separate groups. 56
A.6 Network performance results, considering the Rician fast-fading component, for 5 GUS in 2 separate groups. 57
A.7 Network performance results, considering the Rician fast-fading component, for 10 GUS in 2 separate groups. 57

List of Tables

4.1 Network parameters. 30
4.3 UAV and environment parameters. 30
4.2 Relation between minimum targeted SNR and expected Data Rate for a number of ground users equal to N, considering the IEEE 802.11ac technology and 160 MHz channel bandwidth. 31

5.1 Simulation parameters. 38

Abbreviations and Symbols

3D	Three-Dimensional
AFG	Attractive PF Generator
CCDF	Complementary Cumulative Distribution Function
CDF	Cumulative Distribution Function
CoDeL	Controlled Delay
CS	Central Station
CSMA/CA	Carrier Sense Multiple Access with Collision Avoidance
DDPG	Deep-Deterministic Policy Gradient
EPAP	Energy and Performance Aware Relay Positioning
EREP	Energy-aware Relay Positioning
FAP	Flying Access Point
FCR	Flying Communications Relay
FN	Flying Network
FSPL	Free-Space Path Loss
GEE	Global Energy Efficiency
GU	Ground User
GW	Gateway
GWP	Gateway UAV Placement
LoS	Line-of-Sight
LSTM	Long Short-Term Memory
MAC	Medium Access Control
MCS	Modulation and Coding Scheme
MUAVE	Multi-UAV Energy Consumption
NIC	Network Interface Card
PF	Potential Fields
QoS	Quality of Service
RFG	Rejective PF Generator
SBG-AC	State-Based Game with Actor–Critic
SNR	Signal to Noise Ratio
SUPPLY	Sustainable multi-UAV Performance-aware Placement
UAV	Unmanned Aerial Vehicle
UE	User Equipment

Chapter 1

Introduction

1.1 Motivation and Problem

In the past few years, there has been an increasing usage of Unmanned Aerial Vehicles (UAVs) for a wide range of applications. Due to their ability to hover over the ground, they are capable of operating almost everywhere. Additionally, they can carry cargo on-board, which makes them suitable platforms for transporting communications nodes, including Wi-Fi Access Points and cellular Base Stations. This has paved way to use Flying Networks (FNs) composed of UAVs, in order to establish and reinforce wireless coverage and network capacity in temporary events. These temporary events include emergency scenarios, such as wild fires and floods, and crowded events, for instance parades and music festivals (Fig. 1.1). When compared with terrestrial networks, FNs impose additional challenges. The UAV placement requires optimizing the Quality of Service (QoS) offered to Ground Users (GUs). Also, since UAVs are not permanently connected to the electrical grid, they rely on on-board power sources, such as electric batteries, for both communications and movement. Considering that the energy supplied by the on-board power sources is quickly consumed, UAVs need to land frequently to recharge their power sources.

Most of the state of the art solutions for UAV placement in FNs are focused on optimizing the QoS offered, neglecting the energy consumed for the propulsion of the UAVs, which limits the time the FN is made available. Recent research work that took into account energy consumption concluded that UAVs are more energy efficient when moving at an optimal speed rather than hovering in a fixed position [2]. Based on this conclusion, some algorithms for defining the UAV trajectory that minimizes its energy consumption without compromising the performance of the FN have been proposed [1]. However, the proposed algorithms are focused on a single UAV. When it comes to multiple UAV placement, most of the state of the art algorithms aim at maximizing the coverege area disregarding that the GUs may have different QoS requirements and may be non-uniformly distributed in the area. One of these works is not energy-aware [6]. The others address the energy-aware UAV placement considering different approaches: 1) to minimize the number of UAVs needed to assure QoS, while positioning the UAVs in hovering [7]; 2) to determine the energy required to assure that the UAVs reach a final destination [9]; 3) to optimize UAV altitude, while positioning the UAVs in hovering [8]; 4) to optimize the three-Dimensional (3D) UAV movement [10]. However, most of them do not allow ensuring heterogeneous QoS requirements for GUs. Minimizing the energy consumption of multiple UAVs, while meeting target QoS levels associated with different GUs, has not been achieved so far. This is the problem addressed in this dissertation.

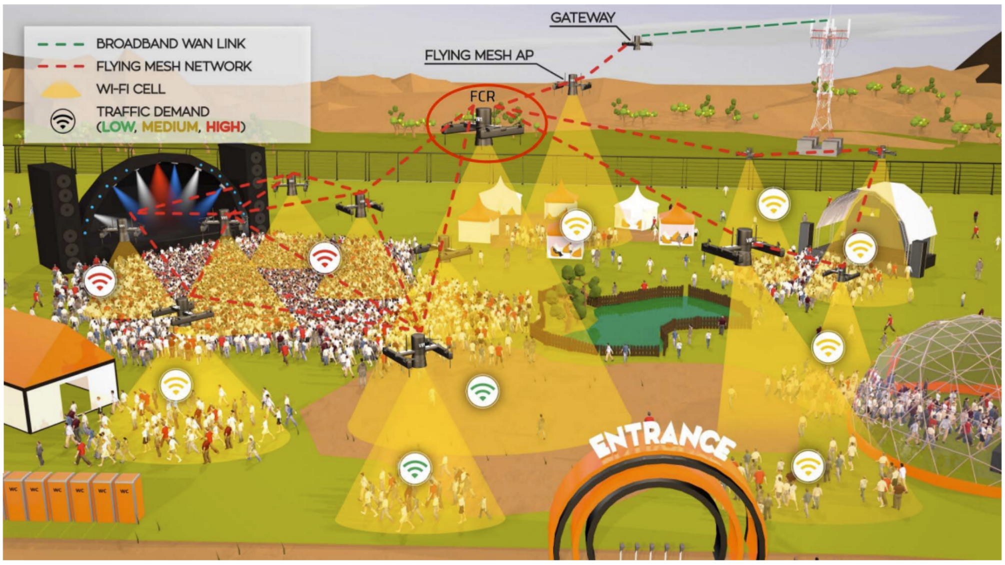

Figure 1.1: Flying Network providing Internet connectivity to the spectators in a music festival [1].

1.2 Objectives

In this dissertation, the main objective was to develop, validate and evaluate an energy-aware placement algorithm to define the optimal trajectories for multiple rotary-wing UAVs that minimize their energy consumption while ensuring the targeted QoS requirements. To achieve this objective the following research challenges were addressed:

- Minimize the number of UAVs required to ensure wireless coverage for all GUs;
- Ensure uninterrupted wireless links with sufficiently high capacity to meet the targeted QoS requirements;
- Avoid collisions between moving UAVs while defining their optimal trajectories.

1.3 Contributions

The main contributions of this dissertation are three-fold:

- The Sustainable multi-UAV Performance-aware Placement (SUPPLY) algorithm, an algorithm that defines the energy-aware positioning for multiple UAVs in a Flying Network, while ensuring the target QoS levels;
- The evaluation of the SUPPLY algorithm in terms of the energy-efficiency gains and the network performance offered.
- The Multi-UAV Energy Consumption (MUAVE) simulator, developed to compute and evaluate the energy consumption of multiple UAVs in an FN.

A conference paper about part of the work developed in this dissertation was published in IJUP 2023.

In addition, a second paper is under preparation to be submitted to a journal.

1.4 Document Structure

This document contains six chapters. In Chapter 2, the state of the art is presented, including the main concepts and related works within the scope of this dissertation. In Chapter 3, the problem statement and his model are presented. The SUPPLY algorithm to solve the problem of this dissertation is detailed. In Chapter 4, the tool developed to compute the multi-UAV energy consumption and evaluate the energy consumption achieved by the SUPPLY algorithm, MUAVE simulator, is presented. In Chapter 5, the validation and evaluation of the SUPPLY algorithm are addressed. The simulation results for energy consumption and network performance are presented. In Chapter 6, a summary of the content of the document, the main conclusions and future work are presented.

Chapter 2

State of the Art

In this chapter, fundamental concepts and state of the art works relevant to address the problem considered in this dissertation are presented. The chapter is divided into four sections. In Section 2.1 a description of the FN concept is presented. In Section 2.2 the energy consumption problem in FNs is analyzed. In Section 2.3 the UAV placement problem in FNs is discussed. Finally, in Section 2.4 the main conclusions drawn from the state of the art review are detailed.

2.1 Flying Networks

In scenarios where the deployment of traditional networks is not feasible or limited, alternative solutions for providing wireless connectivity have to be considered. The use of FNs is a promising solution that has emerged in the literature. The advances in the UAV design associated with electronics miniaturization have allowed UAVs to be more efficient while also becoming lighter and cheaper. For this reason the use of FNs has a continuous increasing interest in the scientific community. The main advantage of FNs is the ability for fast deployment almost everywhere, allowing for on-demand wireless communications in temporary events, such as crowded events and disaster management scenarios. Due to the potential absence of obstacles above the ground, the wireless links between the UAVs that compose the FNs benefit from a strong Line-of-Sight (LOS) component. This simplifies the wireless channel model employed for network planning, making the use of the deterministic Free-Space Path Loss (FSPL) model viable and trustworthy. Moreover, in FNs the positions of the UAVs can be fully controlled and adjusted in 3D space. This paves the way for optimizing the positions of UAVs with the ultimate goal of reducing energy consumption while ensuring target QoS levels.

2.2 Energy Consumption in Flying Networks

Traditional terrestrial network components are directly connected to the electrical grid. On the other hand, UAVs rely on on-board power sources, such as electrical batteries. For this reason, the endurance of UAVs is limited by their batteries' capacity. In the context of FNs, this means that the UAVs need to be replaced while their batteries recharge, in order to provide a continuous communications service to GUs. In an FN, UAVs require energy for two main tasks: 1) communications, including signal processing and transmission; and 2) propulsion, for keeping the UAVs flying, either while moving or hovering. The second task represents the major component when it comes to energy consumption and it is in the order of hundreds of watts; while the former is in the order of watts. Regarding energy consumption for propulsion, three major factors are worthy of being taken into account. In what follows, we analyze each factor in detail.

2.2.1 UAV Flying Speed

The influence of the UAV flying speed in the UAV power consumption is a factor that has been studied by the scientific community. In [2], the relation between the propulsion power consumption and the UAV flying speed is described and a power consumption model is proposed; an explanation of the model is presented in Section 2.2.3. Their authors concluded that UAVs are more energy efficient when they are moving at an optimal constant speed rather than in hovering state. Fig. 2.1 shows that for the UAV speed of 0 m/s, which represents the hovering state, the power consumption is not minimum. With the increase of the UAV speed the power consumption decreases, until reaching a UAV speed value that is considered optimal from the power consumption point of view ($\approx$ 10 m/s), denoted in Fig. 2.1 as V_{me}. For this speed value the UAV endurance is maximized. From this point onwards, the power consumption increases. Besides V_{me}, the authors have defined V_{mr} as the optimal UAV speed that maximizes the total travelling distance.

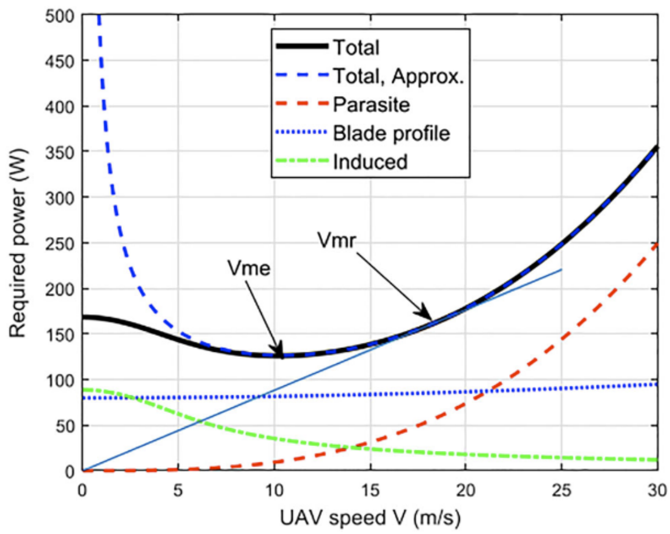

Figure 2.1: Propulsion power consumption versus UAV speed for rotary-wing UAV [2].

2.2.2 UAV Altitude and Payload Weight

In [3], the authors investigated the energy efficient deployment of a UAV, considering both flight dynamics and QoS requirements associated with the users to be served. To formulate the power consumption problem for a UAV in hovering state, several internal and external factors to the UAV were considered. The UAV characteristics, such as the number of rotors and the drag coefficient of the blades, and payload weight constitute the internal factors. The external factors are mainly air resistance and air density. The air density directly depends on the UAV altitude: as the altitude increases the air density decreases. As the altitude increases the UAVs need to increase the induced air velocity in order to keep enough thrust to hover, resulting in more power consumption. To quantify the UAV power consumption when altitude and payload weight change, the authors calculated three power curves for hovering altitudes over Moscow (124m), Ankara (938 m), and Mexico City (2240 m) as a function of payload weight (Fig. 2.2). It is possible to conclude that an increase in altitude or payload weight increases UAV power consumption. As such, both factors should be taken into account when defining the energy-aware positioning of UAVs. Since the problem addressed by this dissertation assumes a constant payload weight for the UAVs, this factor is not considered.

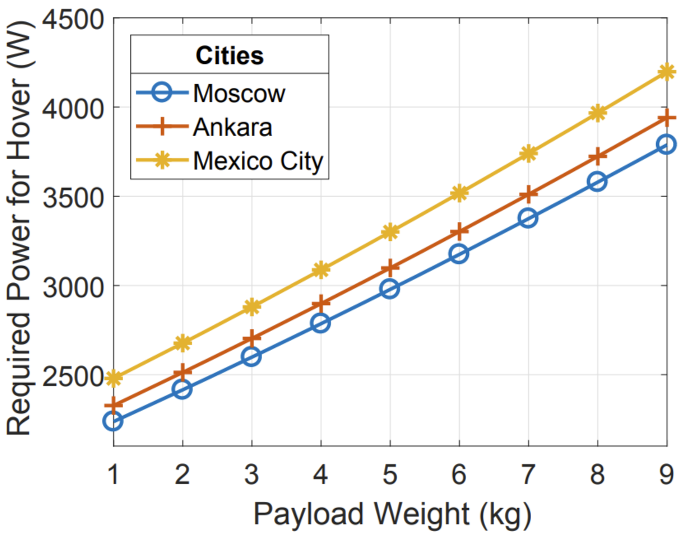

Figure 2.2: Required power to hover over Moscow (124m), Ankara (938 m), and Mexico City (2240 m) as a function of payload weight [3].

2.2.3 Energy Consumption Models

In order to design solutions for defining the energy-aware positioning of UAVs in an FN, an appropriate energy consumption model should be considered. The employed model should be able to replicate the energy consumption of the UAVs in a realistic manner. In the following, the state of the art energy consumption modules for UAVs are presented.

In [2], Zeng et al. derived the power consumption model given by Eq. (2.1) for a rotary-wing UAV; its graphical representation is depicted in Fig. 2.1. This model has been widely used by the scientific community in related works, including in [1], [9], and [10].

$$P(V) = \underbrace{P_0\left(1+\frac{3V^2}{U_{tip}^2}\right)}_{blade\ profile} + \underbrace{P_i\left(\sqrt{1+\frac{V^4}{4v_0^4}}-\frac{V^2}{2v_0^2}\right)^{1/2}}_{induced} + \underbrace{\frac{1}{2}d_0\rho sAV^3}_{parasite} \tag{2.1}$$

In Eq. (2.1), P_0 and P_i are two constants representing the *blade profile power* and *induced power*. In hovering state, U_{tip} is the tip speed of the rotor blade, v_0 is the mean rotor induced velocity, d_0 and s are respectively the fuselage drag ratio and rotor solidity, ρ stands for the air density, and A denotes the rotor disc area. The authors concluded that the propulsion power consumption of rotary-wing UAVs consists of three main components: blade profile, induced, and parasite power. The blade profile power and parasite power increase quadratically and cubically, respectively, with V. These are necessary to overcome the profile drag of the blades and the fuselage drag. Additionally, the induced power is required to overcome the induced drag of the blades, which decreases with V.

Muli et al., in [4], made a comparative overview of different energy consumption models for UAVs. They also proposed a data-driven model based on an original Long Short-Term Memory (LSTM) architecture. This model was designed to fit a realistic data set [13]. From the data set, 21 features were considered, in order to create the energy prediction model. To evaluate the proposed model as well as the state of the art counterparts, the authors applied the same predefined UAV trajectory to all the models. By comparing the obtained energy consumption results with the real energy consumption values for the same UAV trajectory in Fig. 2.3, they concluded that the model created and trained by them is able to fit the real power consumption more accurately than all the other models, as depicted in Fig. 2.4.

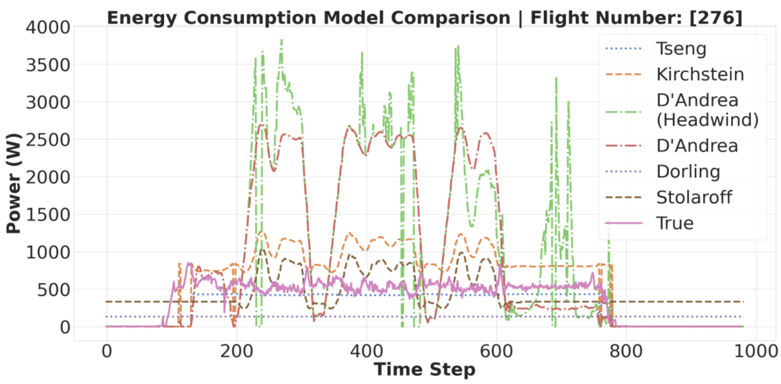

Figure 2.3: Comparison all models for power consumption [4].

Following the evaluation, the authors performed a sensitivity analysis of the trained model, varying the most important parameters for UAV energy consumption: UAV speed, altitude and payload weight. They concluded that payload weight is the characteristic that most influences energy consumption, followed by the speed and the altitude of the UAV. Overall, increasing the payload weight and UAV altitude directly increases the energy consumption. In turn, they concluded that the energy consumption is lower with the increase of UAV speed. These results are

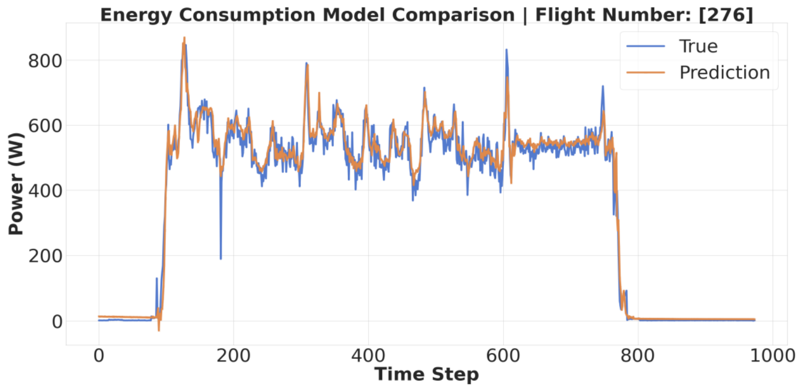

Figure 2.4: Comparison of the proposed LSTM model with the ground truth [4].

depicted in Fig. 2.5. Despite the results regarding the UAV speed may seem contradictory to common sense and when considering other models, it is important to note that the maximum UAV speed considered was 12 m/s. This value is close to the speed that leads to the minimum power required for UAV propulsion, according to the power profile curve depicted in Fig. 2.1. As such, it is expected that high speed values lead to an increase in the power consumption. These conclusions validate the power profile curve depicted in Fig 2.1 and the corresponding model given by Eq. (2.1).

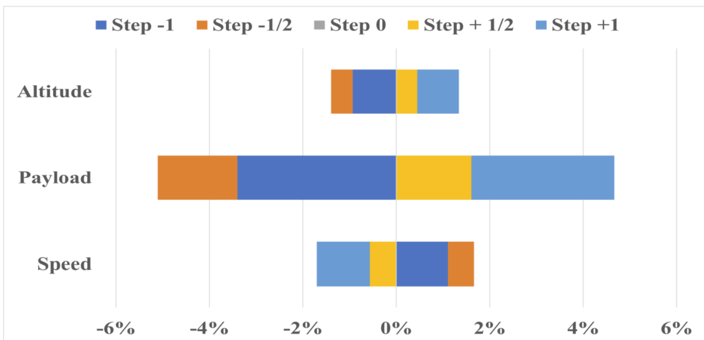

Figure 2.5: Sensitivity of power consumption to key features [4].

More recently, two new UAV energy consumption models that build upon the model given by Eq. (2.1) were proposed in [14] and [12], respectively. These models extend the previously presented model by considering acceleration a relevant factor for the energy consumption of the UAV. The first model considers both centrifugal and tangential acceleration components. The second model considers only the centrifugal acceleration, since the authors concluded that the impact of the tangential acceleration in energy consumption is already reflected in the model by changing the velocity. This model is given by Eq. (2.2).

$$E(q(t)) = \underbrace{\int_0^T P_0 \left(1 + \frac{3||v(t)||^2}{U_{tip}^2}\right) dt}_{blade\,profile} + \underbrace{\int_0^T P_i \sqrt{1 + \frac{{a_c}^2(t)}{g^2}} \left(\sqrt{1 + \frac{{a_c}^2(t)}{g^2} + \frac{||v(t)||^4}{4v_0^4}} - \frac{||v(t)||^2}{2v_0^2}\right)^{1/2} dt}_{induced}$$
$$+ \underbrace{\int_0^T \frac{1}{2} d_0 \rho s A ||v(t)||^3 dt}_{parasite} + \Delta_K \tag{2.2}$$

Where a_c and g represent the centrifugal acceleration and the gravity acceleration, respectively, in addition to the parameters already presented in Eq.(2.1). This model is capable of calculating the energy consumption for an arbitrary 2D flight. Besides introducing the new theoretical energy consumption model presented, the authors also validated the first model given by (2.1) for straight line flight. Furthermore they validated the new model for the specific case of circular flight, using real flight data.

2.3 UAV Placement

Regarding UAV placement, it is possible to group state of the art solutions into single UAV placement (Section 2.3.1) and multi-UAV placement (Section 2.3.2).

2.3.1 Single UAV Placement

In [3], the authors addressed the energy-aware positioning for a single UAV acting as a Flying Access Point (FAP). They considered the communications model depicted in Fig. 2.6, in which a UAV with an antenna beamwidth of 2θ provides wireless communications to users distributed in an arbitrary geographical area. The UAV is set to hover at an altitude of h and it is able to cover k users that are inside a circle of radius R. There is a direct relationship between h and R: increasing h leads to an increase in R. The algorithm aims at defining the position of the UAV that maximizes the number of users covered, while considering the power constraints and also the QoS requirements of the users.

Making use of the algorithm, they defined the optimal height at which the UAV should hover considering different QoS requirements of the users and UAV power constraints. The authors considered a UAV hovering over Moscow (124 m) and three levels of minimum Signal to Noise Ratio (SNR) for the wireless links established between the UAV and the users. Simulation results are depicted in Fig. 2.7. It is possible to conclude that when not considering power constraints the UAV is set to hover at the highest altitude that assures the minimum SNR, in order to maximize the number of users covered. However, power constraints may prevent the UAV to reach the altitude that maximizes coverage. Since the authors do not minimize energy consumption, the UAV is set to hover at the optimal position that maximizes the coverage area. However, positioning the UAV in hovering state neglects that UAVs are more energy efficient while moving at an optimal speed.

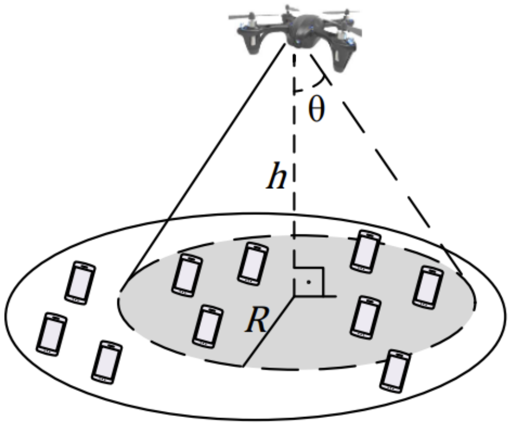

Figure 2.6: UAV Communication Model [3].

Coelho et al. considered in [5] an FN composed of two-tiers: access and backhaul networks. The FN is composed of two types of UAVs: FAPs, which provide Internet access to GUs, and a Gateway (GW) UAV, which forwards data to/from the Internet. The FAP positioning algorithm and the GW UAV positioning algorithm are assumed to run on a Central Station (CS), which is in charge of sending the updated positions to the UAVs. The CS periodically updates the FAPs positioning using the NetPlan algorithm [6] and defines the FAPs' forwarding tables using the RedeFINE algorithm [15]. It is also in charge of updating the GW UAV position to assure the establishment of a backhaul wireless link between with the FAPs. For that purpose, the authors have proposed the Gateway UAV Placement (GWP) algorithm. GWP aims at ensuring target SNR values for the wireless links established between the FAPs and the GW UAV, in order to induce the use of the minimum Modulation and Coding Scheme (MCS) index with a data rate able to accommodate the offered traffic. The FSPL model is used to calculate the SNR, assuming a constant noise power and channel bandwidth. The GWP algorithm defines the maximum distance that assures the targeted SNR for the wireless links between each FAP and the GW UAV. In 3D space this results in a sphere for each FAP with a radius equal to the maximum distance derived. The optimal position for the GW UAV is the subspace defined by the intersection of the resulting spheres for all FAPs in the network. The GW UAV position is reached in an iterative manner, in which the transmission power of the UAVs is successively increased by 1 dBm until a solution is found, considering 0 dBm as the initial transmission power. To evaluate the proposed algorithm, the ns-3 simulator was used. Two different scenarios were considered: scenario A with 4 FAPs organized in a simple distribution (Fig. 2.8a) and scenario B with 10 FAPs randomly positioned in order to form two zones with different traffic demand: λ_1 bit/s and λ_2 bit/s (Fig. 2.8b). The GWP algorithm was evaluated considering two metrics: aggregate throughput and delay. The results obtained confirm that by dynamically defining the position of the GW UAV it is possible to improve the FN performance for the metrics considered. Despite the gains obtained in network performance, the GWP does not take into consideration the energy consumption of the UAVs, making them hover in a fixed position.

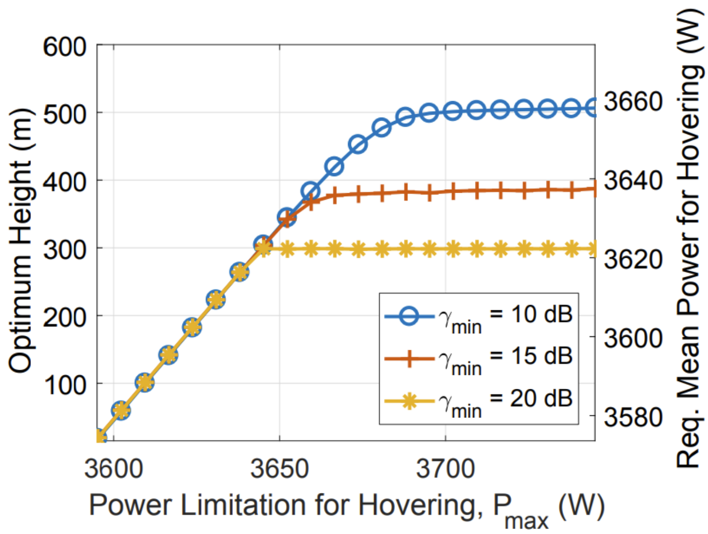

Figure 2.7: Optimum height for different QoS requirements, considering γ_{min} equal to 10, 15 and 20 dB, as a function of the power required for hovering [3].

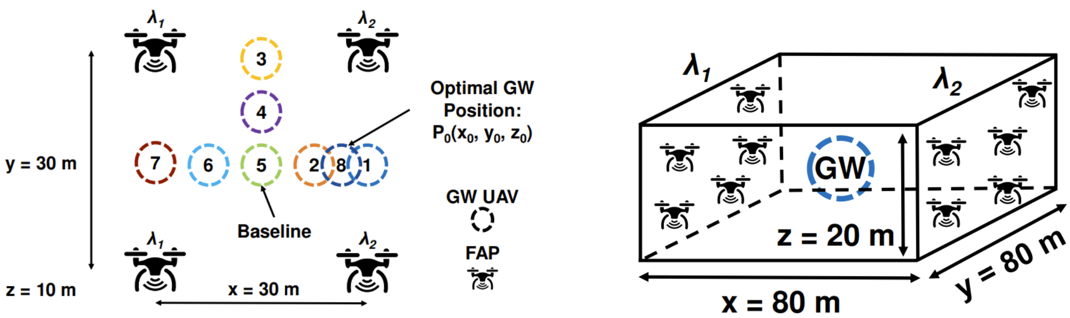

(a) Scenario A. (b) Scenario B.

Figure 2.8: Simulation scenarios considered in the evaluation of the GWP algorithm [5].

Rodrigues et al. proposed in [1] the Energy and Performance Aware Relay Positioning (EPAP) algorithm, a successor of the Energy-aware Relay Positioning (EREP) algorithm proposed by the same authors in [16]. EPAP and EREP aim at defining the trajectory for a Flying Communications Relay (FCR) UAV that minimizes the energy consumption without compromising the QoS offered. The algorithms lie on the energy consumption model defined in Eq. (2.1), which allows to conclude that UAVs are more energy efficient when moving at an optimal speed rather than hovering in a fixed position. Building upon the GWP algorithm [5], EPAP and EREP define the intersection of the spheres that represent the volume within which a minimum SNR is ensured for the wireless links established between all FAPs and the FCR UAV. Considering that changes in altitude are not energy efficient, the FCR UAV moves in a fixed horizontal plane within the intersection volume. Both algorithms assume a maximum transmission power for the UAVs, which allows maximizing the intersection volume, while minimizing the FCR UAV energy consumption, due to a longer trajectory allowed for the FCR UAV. EREP and EPAP only consider the energy consumption for the propulsion of the FCR UAV, since the power used by the Network Interface Cards (NICs) is negligible. After defining the horizontal plane, EPAP and EREP compute three candidate trajectories for the FCR UAV, which consist of a set of waypoints. The trajectory that has the greatest length allows minimizing the UAV energy consumption. The authors concluded that when using EREP and EPAP to define the trajectory of the FCR UAV, the network's performance is not compromised when compared to placing the FCR UAV in hovering state, while the FCR UAV endurance is increased. Moreover, they concluded that the endurance gains decrease with the increase of the number of FAPs used in the FN, due to a resulting smaller intersection volume and consequently a shorter length for the trajectories allowed for the FCR UAV. The EREP and EPAP algorithms considered the UAV movement as a key point for the optimization of its energy consumption. However, the proposed algorithms are only applicable to a single FCR UAV, while multiple UAVs that act as FAPs are placed in hovering, which is not the most energy efficient state. This paves way for evolving EPAP and EREP by proposing an algorithm that allows defining the energy efficient movement for multiple UAVs.

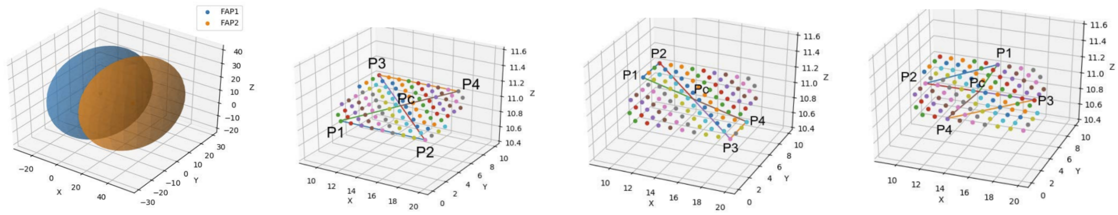

(a) Spheres (b) Trajectory 1 (c) Trajectory 2 (d) Trajectory 3

Figure 2.9: Intersection of the spheres of two FAPs and candidate FCR trajectories defined by EREP/EPAP [1].

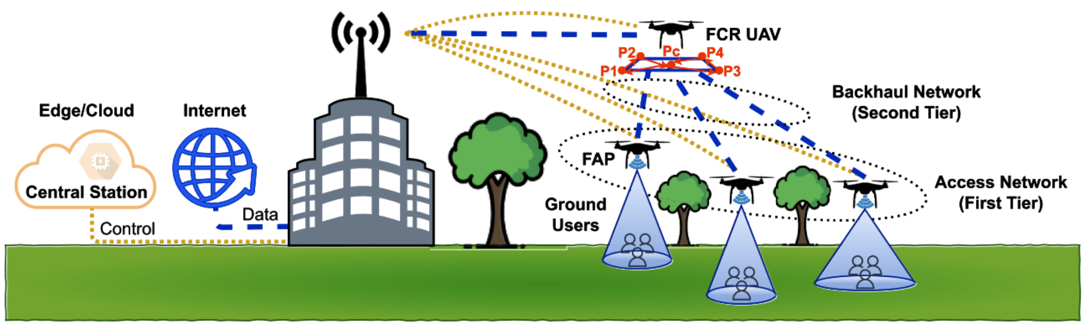

Figure 2.10: Flying network organized into a two-tier architecture. An example trajectory defined by EREP/EPAP to minimize the FCR UAV energy consumption is depicted by the red arrows [1].

In [17], Rodrigues H. discussed the state of the art solutions on gateway positioning in FNs. However, they are focused on the positioning of single UAV acting as a gateway.

2.3.2 Multi-UAV Placement

In [6], the authors proposed the NetPlan algorithm, which dynamically adjusts the horizontal position of the FAPs and the Wi-Fi cell ranges based on the traffic demand of the users, in order to improve the FN's aggregate throughput. The NetPlan algorithm uses the Potential Fields (PF) technique to create force fields that influence the position of the FAPs. They attract FAPs to areas with high traffic demand (Attractive PF Generators (AFGs)) and repel FAPs from areas with low traffic demand (Rejective PF Generators (RFGs)). The FAPs closer to users with high traffic demand establish smaller Wi-Fi cells to improve throughput, while the remaining FAPs establish larger cells to ensure full coverage of the area. The authors obtained the results depicted in Fig. 2.11 for two different scenarios. Moreover, through ns-3 simulation results, the authors concluded that in scenarios of crowded events, the NetPlan algorithm leads to improvements in QoS metrics, especially in terms of mean throughput, without compromising the coverage area. However, NetPlan focuses on optimizing QoS, disregarding energy efficiency.

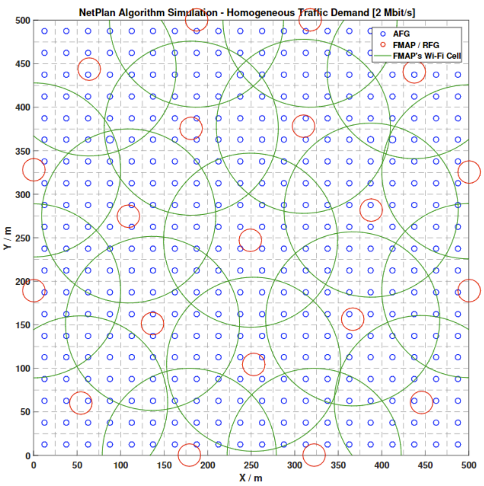

(a) Homogeneous traffic demand.

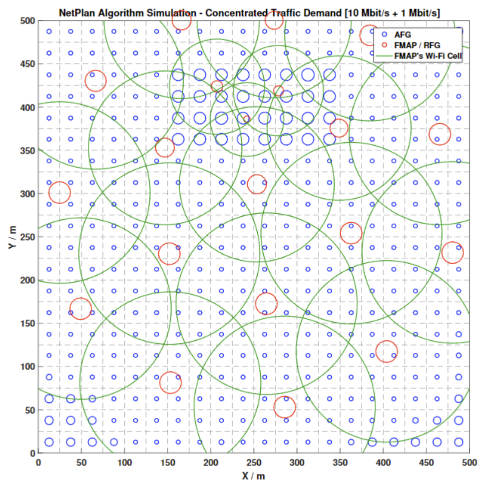

(b) Concentrated traffic demand.

Figure 2.11: NetPlan multi-UAV placement for two scenarios, depicting the AFGs (blue), the FAPs/RFGs (red) and their Wi-Fi cells (green) [6].

The authors of [7] propose SLICER, an algorithm that enables the placement and allocation of communication resources in slicing-aware flying networks. The SLICER algorithm enables the computation of optimal 3D positions for a minimum number of FAPs, based on GUs positions and their QoS requirements. The algorithm ensures that network slices with target QoS levels are made available as required. To achieve the optimal solution, SLICER relies on the state of the art solver Gurobi optimizer [18]. The authors conducted ns-3 simulations for multiple random networking scenarios to evaluate the performance of the flying network when utilizing SLICER. The results demonstrate that the algorithm achieves the targeted QoS levels associated with multiple network slices, while minimizing the utilization of communication resources. However, in spite of the FAPs being positioned in their optimal positions to assure QoS to the GUs, they are placed in hovering, which is not the most energy efficient state.

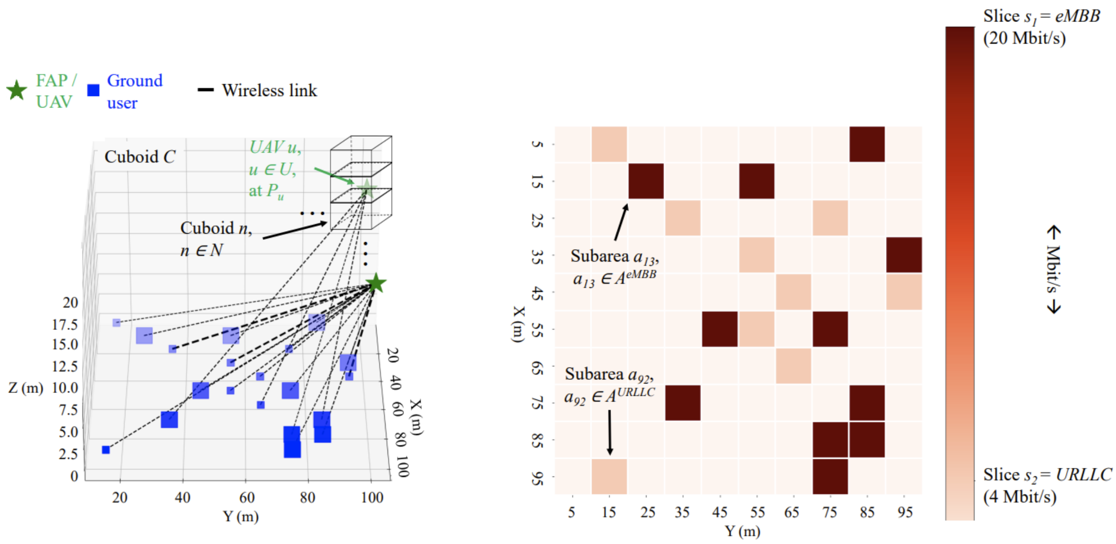

Figure 2.12: SLICER result for a networking scenario composed of multiple GUs (blue squares) served by two FAPs (green stars). The GUs are associated with two network slices made available in different subareas. [7]

Babu et al. [8] proposed a 3D placement algorithm for multiple UAVs. The FAPs, are set to hover in a fixed position. Both vertical and horizontal positioning are defined in order to maximize the Global Energy Efficiency (GEE), ratio between the total number of successfully transmitted bits by all the User Equipments (UEs) and the total energy consumption. As the altitude increases, the coverage area ensured by the UAVs increases while the UAV energy consumption also increases, reducing GEE. For the horizontal positioning, the higher the coverage area the higher the GEE. Taking this into account, the vertical position is defined by solving the GEE maximization problem for a single FAP, which results in the most energy-efficient hovering altitude. The area covered by a FAP is defined as a circular cell, while the interference between adjacent cells is defined as inter-cell interference. After defining the vertical positioning for a single FAP, the horizontal positioning for multiple FAPs is defined by maximizing the total coverage area, while reducing inter-cell interference; this is achieved by avoiding cell overlapping. Considering multiple FAPs with the same coverage areas, the problem consists in maximizing the packing density of the FAPs coverage areas. This horizontal positioning problem takes the form of a circle packing problem for maximum packing density, maximizing the number of circles inside a given area, and is solved using an algorithm that iteratively places layers of circles from the edge of the area to the center. The output of the algorithm for two different sizes of areas to be covered is depicted in Fig. 2.13. The cells represented in green were the first determined followed by the cells in red. The algorithm maximizes the wireless coverage represented by means of ground areas, whose radius could be defined to ensure a target SNR between the UAV and the users. Despite defining the altitude at which the UAVs should be placed in order to be more energy efficient (energy consumption increases for higher altitudes), the authors consider that the UAVs should be hovering in a specific position. However, UAVs are more energy efficient when they are moving at a constant optimal speed rather than in hovering state, as referred to in Section 2.2.1.

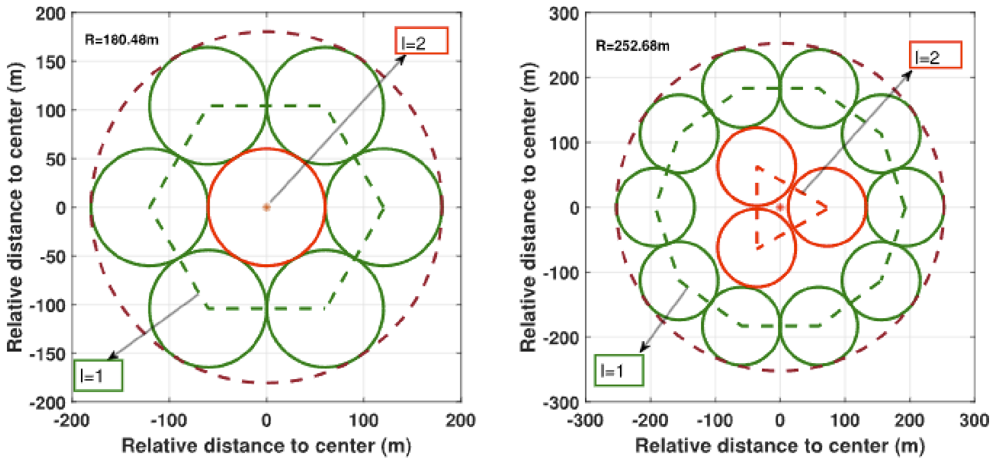

Figure 2.13: Horizontal Positioning of FAPs [8].

Tuan Do et al. proposed in [9] an energy efficient approach for multi UAV placement. The goal was to maximize the UAV's service time and downlink throughput by using a deep-reinforcement learning method called Deep-Deterministic Policy Gradient (DDPG). The authors considered multiple rotary-wing UAVs, a set of GUs and two charging stations. The UAVs should leave the first charging station, assure service to GUs, and reach the other charging station without running out of energy. To make sure the UAV has enough energy to reach the charging station, the energy available in the battery and needed to reach the charging station is calculated, using the energy model given by Eq. 2.1. The algorithm follows a best-effort approach to maximize the downlink throughput, while trying to ensure the minimum required rate for each GU. At each time step, the algorithm tries to achieve the optimal solution by defining the trajectory design and transmission power for each UAV. For that purpose, it considers the positions of: UAVs, GUs, and charging stations. To assess the proposed algorithm the authors carried out simulations for 2 UAVs, 10 GUs uniformly distributed, and 2 charging stations randomly positioned. The UAVs were set to travel and hover at an altitude of 100 m with the maximum possible speed of 60 m/s. However, the energy efficiency problem is not addressed, since the energy used by the UAVs to reach a charging station is not minimized. Moreover, the UAVs movement is not energy-aware, since they can be set hover over users and travel at non-optimal speeds for improving the overall downlink throughput.

In [10], Nemer et al. proposed an energy-efficient UAV movement control model for fair communications coverage. The model divides an area to be covered into different cells, where the center of each cell is referred to as the point of interest which corresponds to a user. The UAVs should move in order to maximize coverage (number of cells covered) and fairness (homogeneously covering all the cells) while minimizing energy consumption. The authors proposed a novel algorithm, called State-Based Game with Actor–Critic (SBG-AC) to control multiple UAVs

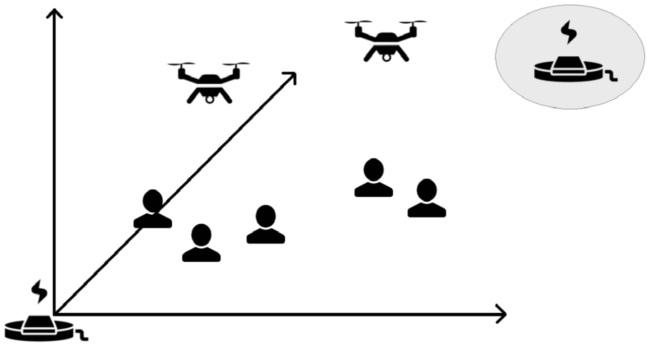

Figure 2.14: Multi-UAV Wireless Communications System [9].

in the network. To solve the movement control problem for a group of UAVs under fairness, coverage, and energy constraints, they formulated the problem as a state-based potential game. The algorithm solves the formulated problem and guarantees the convergence of the model. In the SBG-AC model, each UAV acts as an agent that searches and learns its 3D location policy. Simulation results demonstrated the efficiency of SBG-AC, which enables better performance compared to other deep reinforcement learning methods. The approach tries to minimize UAV energy consumption. However, regarding UAV placement, it aims at maximizing the cells covered, considering that they are equally sized and designed to serve a user in its center. The model does not consider non-uniform positioning of the users and different QoS requirements.

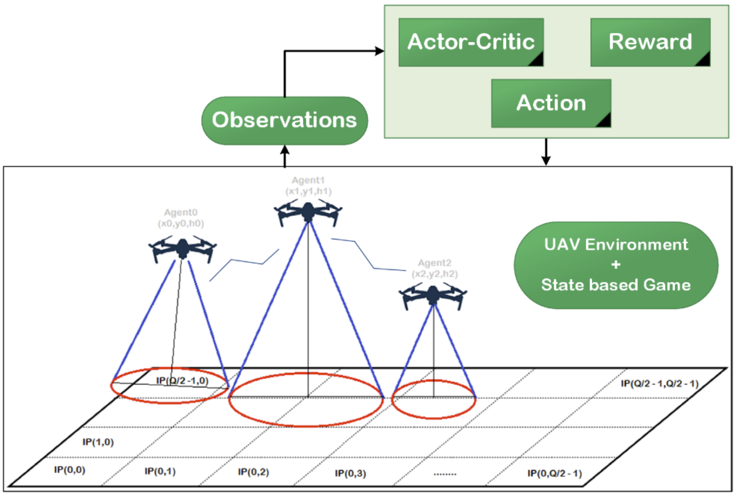

Figure 2.15: UAV network with the actor–critic algorithm [10].

In [19], the authors present a comprehensive survey on UAV-assisted wireless networks. The paper provides an overview of solutions for several problems in multiple network architectures and technologies involving UAVs. Moreover, it points out the challenges imposed by FNs, including UAV energy efficiency. However, the state of the art solutions presented to address the UAV energy efficiency challenge focus on optimizing the energy used for communications. Regarding multi

UAV placement, none of the solutions presented defined a UAV energy efficient movement, while assuring different QoS requirements. This is still an open research challenge.

2.4 Summary

After analysing the state of the art works relevant for this dissertation it is possible to conclude that there is an increasing interest of the scientific community in using FNs as an approach to guarantee wireless connectivity in temporary events. However, there are challenges to be addressed in the use of FNs, particularly in terms of energy efficiency. UAVs can be positioned in 3D space but have energy limitations. Factors such as UAV flying speed, UAV altitude, and payload weight influence the UAV energy consumption, with higher UAV altitude and payload weight resulting in increased energy consumption. Regarding the UAV flying speed, it was found that UAVs are more energy efficient moving at an optimal speed rather than hovering. While there are solutions that optimize the movement of a single UAV to reduce energy consumption, they are not suitable for multiple UAVs. For the case of multi-UAV placement, existing solutions focus on maximizing coverage area without considering the non-uniform distribution of users and heterogeneous QoS requirements. A solution for multi-UAV placement that addresses the energy efficient UAV movement, while enabling heterogeneous QoS requirements, has not been proposed so far.

Chapter 3

Sustainable multi-UAV Performance-aware Placement Algorithm

Considering the survey of state of the art work presented in Chapter 2, this chapter explains the solution proposed to solve the problem addressed in this dissertation.

3.1 Problem Statement

To develop an algorithm for the placement of multiple rotary-wing UAVs acting as FAPs, we need to take into consideration the location and the traffic offered by each Ground User (GU), in order to assure the targeted QoS levels. UAVs are not permanently connected to the electrical grid; they rely on on-board power sources, such as electric batteries, with limited capacity. As such, the UAVs endurance is limited by their batteries' capacity. Considering that the energy supplied by the batteries is quickly consumed, UAVs need to land frequently to recharge their battery. For this reason, the maximum UAV endurance should be guaranteed to maximize the network availability and ensure the target QoS levels without loss of connectivity. Since UAV propulsion represents the major component of the energy consumed by a UAV, an energy efficient movement should be defined. This dissertation solves the joint energy and performance aware placement of multiple UAVs, in order to minimize the UAV energy consumption while ensuring target QoS requirements for the GUs.

3.2 System Model and Problem Formulation

We consider the network architecture depicted in Fig. 3.1. The network is composed of a CS, multiple FAPs and multiple GUs.

- **Central Station (CS)**: Responsible for monitoring the state of the network and controlling the placement of the UAVs.
- **Flying Access Points (FAPs)**: Rotary-wing UAVs acting as access points, providing a radio access network to GUs. They receive up-to-date placement information from the CS and reposition themselves accordingly.
- **Ground Users (GUs)**: Users on the ground that seek network access. GUs can have heterogeneous QoS requirements.

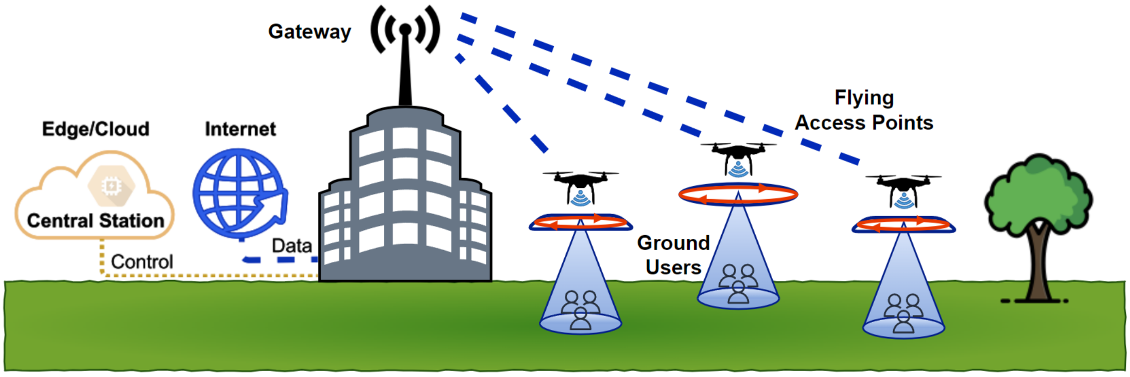

Figure 3.1: Network architecture considered in this dissertation.

The problem is focused on defining energy and performance aware trajectories for multiple FAPs. To offer different QoS requirements, high enough capacity must be ensured by each wireless link established between the GUs and the FAPs. We assume that the maximum channel capacity is equal to the data rate associated with the Modulation and Coding Scheme (MCS) index selected by the Medium Access Control (MAC) automatic rate mechanism. To achieve higher channel capacities in the wireless links the value of SNR also needs to be higher, as depicted in Fig. 3.2. SNR represents the ratio between the power of the received signal (P_r) over the power of background noise (N_0), as given by Eq. (3.1). The SNR value can be defined in three ways: increasing the transmission power, decreasing the power of background noise, and defining a suitable distance between the communications nodes. Assuming a constant channel bandwidth, the background noise is not controllable in this environment; we consider it is constant.

$$SNR = \frac{P_r}{N_0} \tag{3.1}$$

The LoS component is assumed to be strong between the elements of the network, especially due to the potential lack of obstacles induced by the UAV altitude. As such, the FSPL model [20] is considered to calculate the power received, as defined in Eq (3.2).

$$\frac{P_r}{P_t} = \left[\frac{\lambda}{4\pi d}\right]^2 \tag{3.2}$$

HT MCS	VHT MCS	Modulation	Coding	20MHz Data Rate 800ns	20MHz Data Rate 400ns	20MHz Min. SNR	20MHz RSSI	40MHz Data Rate 800ns	40MHz Data Rate 400ns	40MHz Min. SNR	40MHz RSSI	80MHz Data Rate 800ns	80MHz Data Rate 400ns	80MHz Min. SNR	80MHz RSSI	160MHz Data Rate 800ns	160MHz Data Rate 400ns	160MHz Min. SNR	160MHz RSSI
1 Spatial Stream																			
0	0	BPSK	1/2	6.5	7.2	2	-82	13.5	15	5	-79	29.3	32.5	8	-76	58.5	65	11	-73
1	1	QPSK	1/2	13	14.4	5	-79	27	30	8	-76	58.5	65	11	-73	117	130	14	-70
2	2	QPSK	3/4	19.5	21.7	9	-77	40.5	45	12	-74	87.8	97.5	15	-71	175.5	195	18	-68
3	3	16-QAM	1/2	26	28.9	11	-74	54	60	14	-71	117	130	17	-68	234	260	20	-65
4	4	16-QAM	3/4	39	43.3	15	-70	81	90	18	-67	175.5	195	21	-64	351	390	24	-61
5	5	64-QAM	2/3	52	57.8	18	-66	108	120	21	-63	234	260	24	-60	468	520	27	-57
6	6	64-QAM	3/4	58.5	65	20	-65	121.5	135	23	-62	263.3	292.5	26	-59	526.5	585	29	-56
7	7	64-QAM	5/6	65	72.2	25	-64	135	150	28	-61	292.5	325	31	-58	585	650	34	-55
	8	256-QAM	3/4	78	86.7	29	-59	162	180	32	-56	351	390	35	-53	702	780	38	-50
	9	256-QAM	5/6			31	-57	180	200	34	-54	390	433.3	37	-51	780	866.7	40	-48
2 Spatial Streams																			
8	0	BPSK	1/2	13	14.4	2	-82	27	30	5	-79	58.5	65	8	-76	117	130	11	-73
9	1	QPSK	1/2	26	28.9	5	-79	54	60	8	-76	117	130	11	-73	234	260	14	-70
10	2	QPSK	3/4	39	43.3	9	-77	81	90	12	-74	175.5	195	15	-71	351	390	18	-68
11	3	16-QAM	1/2	52	57.8	11	-74	108	120	14	-71	234	260	17	-68	468	520	20	-65
12	4	16-QAM	3/4	78	86.7	15	-70	162	180	18	-67	351	390	21	-64	702	780	24	-61
13	5	64-QAM	2/3	104	115.6	18	-66	216	240	21	-63	468	520	24	-60	936	1040	27	-57
14	6	64-QAM	3/4	117	130.3	20	-65	243	270	23	-62	526.5	585	26	-59	1053	1170	29	-56
15	7	64-QAM	5/6	130	144.4	25	-64	270	300	28	-61	585	650	31	-58	1170	1300	34	-55
	8	256-QAM	3/4	156	173.3	29	-59	324	360	32	-56	702	780	35	-53	1404	1560	38	-50
	9	256-QAM	5/6			31	-57	360	400	34	-54	780	866.7	37	-51	1560	1733	40	-48
3 Spatial Streams																			
16	0	BPSK	1/2	19.5	21.7	2	-82	40.5	45	5	-79	87.8	97.5	8	-76	175.5	195	11	-73
17	1	QPSK	1/2	39	43.3	5	-79	81	90	8	-76	175.5	195	11	-73	351	390	14	-70
18	2	QPSK	3/4	58.5	65	9	-77	121.5	135	12	-74	263.3	292.5	15	-71	526.5	585	18	-68
19	3	16-QAM	1/2	78	86.7	11	-74	162	180	14	-71	351	390	17	-68	702	780	20	-65
20	4	16-QAM	3/4	117	130	15	-70	243	270	18	-67	526.5	585	21	-64	1053	1170	24	-61
21	5	64-QAM	2/3	156	173.3	18	-66	324	360	21	-63	702	780	24	-60	1404	1560	27	-57
22	6	64-QAM	3/4	175.5	195	20	-65	364.5	405	23	-62			26	-59	1580	1755	29	-56
23	7	64-QAM	5/6	195	216.7	25	-64	405	450	28	-61	877.5	975	31	-58	1755	1950	34	-55
	8	256-QAM	3/4	234	260	29	-59	486	540	32	-56	1053	1170	35	-53	2106	2340	38	-50
	9	256-QAM	5/6	260	288.9	31	-57	540	600	34	-54	1170	1300	37	-51			40	-48

Figure 3.2: MCS index information for the IEEE 802.11ac technology [11].

In Eq. (3.2), P_r is the received power, P_t is the transmission power, d is the Euclidean distance between the transmitter and the receiver nodes, and λ is the wavelength. The received power falls off in inverse proportion to the square of the distance d between the transmitter and the receiver. Considering a constant P_t, a constant P_r can be ensured by defining a suitable distance d.

We assume the wireless medium is shared and every FAP and GU can listen to each other. The fair share is determined by establishing the maximum capacity of the wireless link between each GU and the FAPs. This capacity is assumed to be equal to the data rate associated with the used MCS index divided by the number of GUs sharing the medium. Considering these conditions, we use the Carrier Sense Multiple Access with Collision Avoidance (CSMA/CA) mechanism for MAC.

In order to calculate the FAPs energy consumption, we use a state of the art energy consumption model, which is defined in Eq. (2.2). As referred to in Section 2.2.1, UAVs are more energy efficient while moving at an optimal speed. This optimal speed depends on the type of trajectory that the UAV is following. For the particular case of circular movement it is possible to obtain the power consumption model defined in Eq. (3.3) from the model given by Eq. (2.2). Letting $a_c = \frac{V^2}{r}$ and $||v(t)|| = V$, where r denotes the circular radius and V the flying speed.

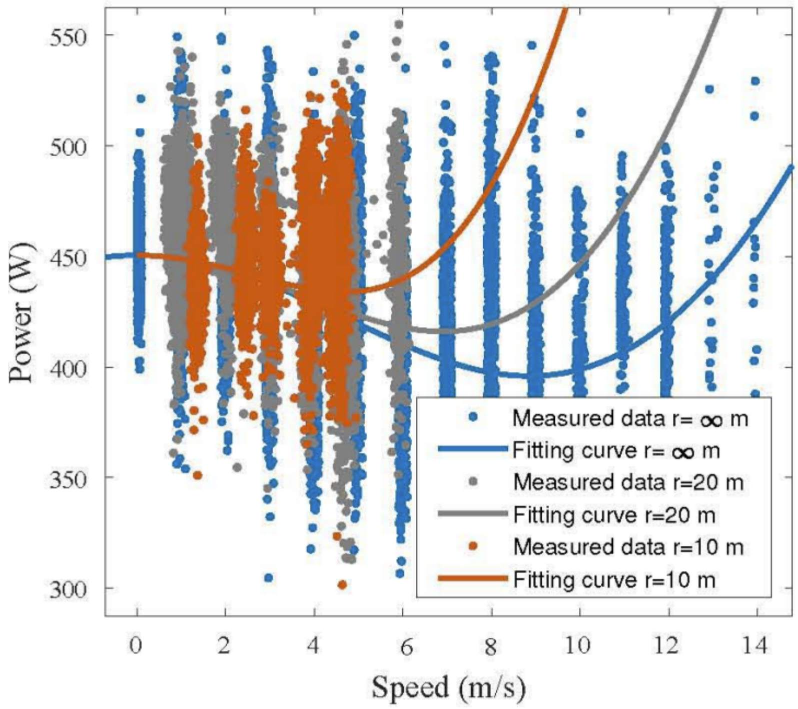

Figure 3.3: Fitting curves of power consumption in circular flight for a rotary-wing UAV [12].

$$P(V,r) = \underbrace{P_0\left(1+\frac{3V^2}{U_{tip}^2}\right)}_{blade\,profile} + \underbrace{P_i\sqrt{1+\frac{V^4}{r^2g^2}}\left(\sqrt{1+\frac{V^4}{r^2g^2}+\frac{V^4}{4v_0^4}}-\frac{V^2}{2v_0^2}\right)^{1/2}}_{induced} + \underbrace{\frac{1}{2}d_0\rho sAV^3}_{parasite} \tag{3.3}$$

As given by Eq. (3.3), the power consumption depends on the flying speed and the circular radius. For each given circular radius there will be a corresponding optimal speed that leads to a minimum power consumption. It is observed that the power consumption increases and that the optimal speed decreases with the decrease of the radius, as depicted in Fig. 3.3. For the case of straight line movement (where the radius approaches infinity) the optimal speed will be at the highest value. Moreover the minimum power consumption will be at is lowest value. Based on this it is possible to conclude that having the FAPs moving in a straight line at the optimal speed allow minimizing the energy consumption. However, using this model we are also able to obtain the optimal speed and calculate the power consumption for curved trajectories with well defined radiuses. This becomes especially relevant since the FAPs need to be at a maximum defined distance to assure a QoS-aware coverage to the GUs, restricting them to a limited area.

The FN is modeled as follows, for any time t of activation. $G = \{GU_1, ...GU_N\}$ is the set of GUs, where N is the number of GUs positioned at $Q_i = (x_i, y_i, 0)$, $F = \{FAP_1, ...FAP_M\}$ is the set of FAPs, where M is the number of FAPs positioned at $Q_j(t) = [x_j(t), y_j(t), z_j(t)]$, and $L \subseteq G \times F$ is the set of directional links between GUs i and FAPs j, with $(i, j) \in L$, $i \in G$ and $j \in F$.

Let us assume that each GU_i, transmits a traffic flow $T_{i,j}$ towards FAP_j, $j \in F$. Each GU_i can only use a single wireless link $L_{i,j}$. Our objective is to minimize the number M of FAPs and to determine trajectories $Q_j(t) = [x_j(t), y_j(t), z_j(t)]$ of each FAP_j, so that the energy consumed by all FAPs is minimal and the transfer of each traffic flow $T_{i,j}$ with data rate $B_{i,j}$, in bit/s, is guaranteed. With this in mind, a wireless link with high enough capacity $C_{i,j}(t)$, to accommodate $B_{i,j}$ must be guaranteed between each GU_i and a FAP_j. Also the aggregate capacity of the wireless links must be lower than or equal to the maximum capacity C^{MAX}.

$$minimize \sum_{j=1}^{M} \int_0^t P_j(t)dt \tag{3.4a}$$

Subject to:

$$P_j(t) \leq P_j^{MAX}, \forall t \tag{3.4b}$$

$$Q_k(t) \neq Q_l(t), \forall k,l \in F, \forall t \tag{3.4c}$$

$$z_j \geq 0, \forall j \in F \tag{3.4d}$$

$$\sum_{j=1}^{M} L_{i,j} = 1, \forall i \in G \tag{3.4e}$$

$$0 \leq B_{i,j}(t) \leq C_{i,j}(t), \forall i \in G, \forall j \in F, \forall t \tag{3.4f}$$

$$\sum_{i=1}^{N} C_{i,j}(t) \leq C^{MAX}, \forall j \in F, \forall t \tag{3.4g}$$

3.3 Sustainable multi-UAV Performance-aware Placement Algorithm

In order to solve the problem formulated in section 3.2, we propose the Sustainable multi-UAV Performance-aware Placement (SUPPLY) algorithm. Considering networking scenarios where the GUs are randomly distributed in a given area, SUPPLY is able to group the GUs to minimize the number of FAPs needed. Furthermore, it defines energy efficient trajectories for the FAPs. SUPPLY algorithm builds upon the SLICER and EREP algorithms proposed in [7] and [16], respectively. It builds upon these two algorithms when it comes to:

- Minimizing communications resources in terms of the number of FAPs needed to assure the target QoS requirements.
- Defining trajectories for the FAPs that minimize the power consumed, without compromising QoS.

The SUPPLY algorithm is divided into two main parts. The first part is in charge of grouping the GUs so that the number of FAPs needed is minimized. The second part allows defining energy efficient trajectories for the FAP serving each formed group, without compromising network performance.

Algorithm 1 SUPPLY Algorithm

```
1:  for all Possible FAP positions do
2:      Calculate SNR values between the GUs and all the possible FAP positions
3:      Estimate the data rate in the links
4:  end for
5:  Solve optimization problem: Groups of GUs ← Solver (GUs positions, possible FAP posi-
    tions, GUs data rate demand, data rate in the links)
6:  for all Groups of GUs do
7:      Define a minimum targeted SNR for each GU
8:      Calculate the maximum Euclidean distance that ensures the targeted SNR for each GU
9:      Calculate intersection area
10:     if Intersection area overlaps previous calculated intersection's areas then
11:         Remove overlapped area from intersection area
12:     end if
13:     Define the centroid of the intersection area
14:     Define the perimeter of the intersection area
15:     Define Circular trajectory
16:     Define Oval Circular trajectory
17:     Define Oval Area trajectory
18:     Choose the most energy efficient trajectory
19: end for
```

The initial step consists in calculating the SNR values for the links between the GUs and all the possible FAP positions (Line 2 of Alg. 1). To calculate the SNR values, we assume a transmission power of 20 dBm for all the nodes. The FAPs are expected to be placed as close to the ground as possible, since it has been demonstrated in the literature that higher altitudes lead to increased power consumption, as explained in section 2.2.2. Moreover, placing the FAPs close to the GUs allows improving the SNR. However, we also have to factor in the interference it may cause to the GUs. We consider a fixed altitude of 6 meters for the FAPs, in order to avoid collisions with people and obstacles on the ground. Considering a fixed altitude also allows reducing complexity by considering a lower number of possible FAP positions. SUPPLY also takes as input a distance step that is used to define all the possible FAP positions. We are considering a step of 1 meter to achieve better precision. This is important to assure that GUs are grouped in the optimal way and the number of FAPs used is minimized. The calculated SNR values are then used to define the data rate in the links by correlating them to the minimum data rate provided by the MCS index table (Line 3 of Alg. 1). The algorithm takes the information from GUs positioning, the possible FAPs positioning, the GUs data rate demand and the data rates obtained for all the links with the FAPs, and outputs the grouping solution that minimizes the number of required FAPs. This is an optimization problem. In its current version, SUPPLY employs, the state of the art solver Gurobi optimizer, [18] (Line 5 of Alg. 1) to solve the optimization problem. However, other state of the art solvers may be considered. During this step, SUPPLY ensures that each GU can be served by a FAP. The results of this part are depicted in Fig. 3.4. This 3D image shows the GUs and the FAPs in their respective positions as well the links between them. The FAP positions shown are

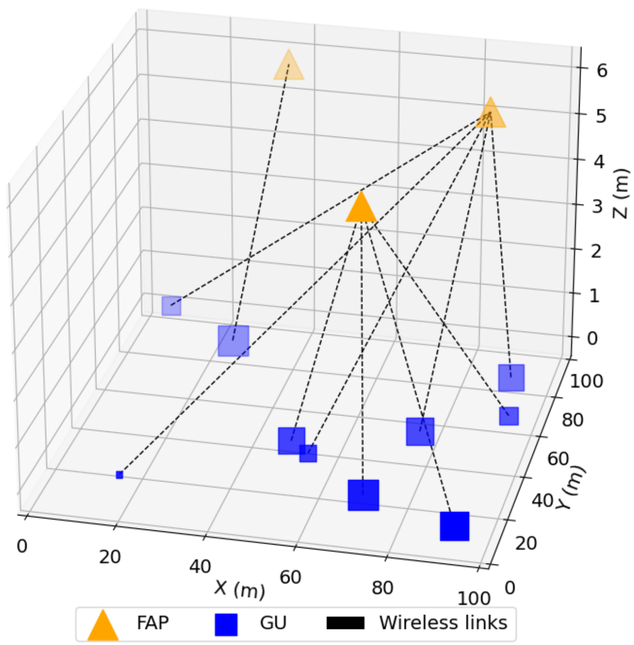

Figure 3.4: Example of grouping result for a 10 GUs scenario. The GUs are represented by blue squares and the FAPs by orange triangles. The doted lines indicate wireless links between the nodes.

preliminary. The ideal positions and energy efficient trajectories are calculated in the second part.

SUPPLY defines the maximum distance that allows inducing a targeted SNR for the wireless links established with the FAPs (Lines 7 and 8 of Alg. 1). In 3D space this results in a sphere for each GU with radius equal to the maximum distance defined. The optimal position for each FAP is the subspace defined by the intersection of the spheres associated with all GUs served by the FAP. Considering that altitude variations are not energy efficient, the FAPs should move within the subspace at a fixed altitude. The altitude should be chosen in such a way that considers the plane of the intersection volume that maximizes the resulting intersection area is considered (Line 9 of Alg. 1). The increased area allows to define more efficient trajectories to be completed by the FAP, leading to reduced energy consumption. Since the GUs are on the ground (altitude equal to 0 meters), the resulting intersection areas decrease with the increase in altitude. In SUPPLY, we consider a minimal altitude of 6 meters. The SUPPLY algorithm assures that the resulting intersection areas do not overlap, in order to avoid collisions between FAPs. For that purpose, any overlapped areas are removed (Lines 10 and 11 of Alg. 1). The ideal position for each FAP is the centroid of the corresponding intersection area (Line 13 of Alg. 1). This is the position considered for the case of the hovering state. Additionally, the perimeter of the intersection area is also delineated, as it is crucial to establish the new trajectories in conjunction with the centroid (Line 14 of Alg. 1). After finding the intersection's areas and their respective centroid and perimeter, the SUPPLY algorithm defines 3 possible trajectories: Circular, Oval Circular and Oval Area (Lines 15, 16 and 17 of Alg. 1). These trajectories can now be power characterized, since the SUPPLY algorithm utilizes the power consumption model given by Eq. (3.3). Examples for the 3 trajectories are depicted in Fig. 3.5. The first trajectory defined is the Circular trajectory. The SUPPLY algorithm defines the radius of the circular trajectory as being the minimum distance from the area's centroid to the perimeter. Then, by varying the angle a circular trajectory is achieved. Following this approach assures that the FAP always remains within the designated area. The second trajectory is named Oval Circular, as its shape closely resembles an oval and it is defined within the circumference determined by the previously calculated circular trajectory. This trajectory is also centered at the area's centroid and is composed of 2 straight line segments and 2 semi-circles, with a radius of 30% of the radius used to define the circular trajectory. The radius for the semi-circles was chosen in this manner to keep the trajectory proportional to size of the limiting area. Also, for testing purposes, smaller percentages were tested and proven to increase energy consumption. The trajectory follows the orientation of the straight line segment connecting the farthest apart perimeter points. For the cases where the area is not circular, this implies that any FAP does not reach the perimeter. This approach has the potential to enhance network performance. The last trajectory is referred to as Oval Area. Unlike the Oval Circular, this trajectory is not confined to the circumference of the Circular trajectory. Instead, it utilizes all the area to maximize the straight line movement. This trajectory shares a similar formation with the Oval Circular trajectory. In line with the previous trajectory, it is also composed of 2 straight line segments and 2 semi-circles and also follows the orientation of the straight line segment connecting the farthest apart perimeter points. However, it is centered in the middle of this straight line segment instead of the area's centroid. Furthermore, the radiuses of the semi-circles are given by the smallest distance between the straight line segment and the closest perimeter point, excluding the two used to form the straight line segment. This assures that the FAP never leaves the area. If the intersection area is too small, not allowing the creation of the trajectories, then the FAP is set to hovering in the ideal position.

The SUPPLY algorithm then chooses the trajectory that leads to better energy efficiency gains: the trajectory with the least energy consumption (Line 18 of Alg. 1).

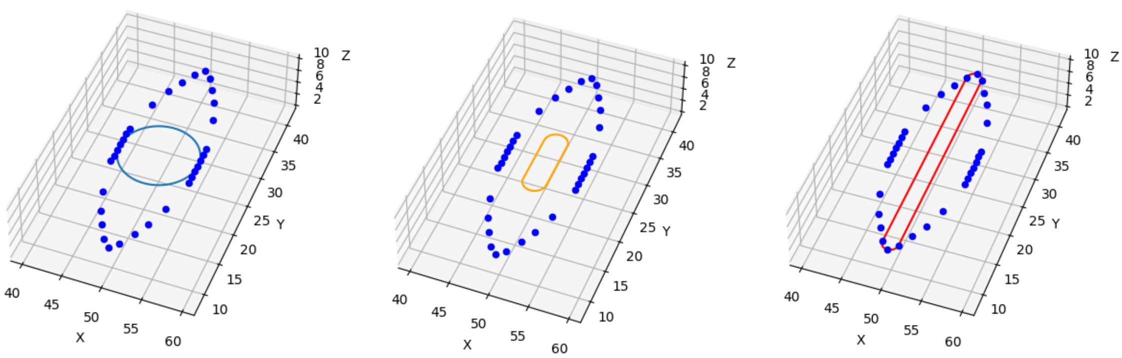

(a) Circular trajectory. (b) Oval Circular trajectory. (c) Oval Area trajectory.

Figure 3.5: Intersection area perimeter and SUPPLY trajectories.

3.4 Summary

In this chapter, the problem addressed in this dissertation was stated, which involves the placement of multiple FAPs to serve multiple GUs while minimizing energy consumption and maintaining overall network performance. The system architecture and its elements, including the Central Station, multiple FAPs, and multiple GUs, were then described. Considering the proposed system model, the problem was formulated and the power consumption model used in the study was presented. Finally, the Sustainable multi-UAV Performance-aware Placement (SUPPLY) algorithm, proposed in this dissertation, was detailed.

Chapter 4

Multi-UAV Energy Consumption Simulator

This chapter presents the Multi-UAV Energy Consumption (MUAVE) simulator. In order to compute the multi-UAV energy consumption in the SUPPLY algorithm presented in Chapter 3 and evaluate the FN's energy efficiency, the MUAVE simulator was developed. MUAVE was implemented in Python [21] building upon the UAV Power Simulator proposed by Rodrigues H. in [22] for computing the power consumption for a single UAV acting as a gateway for a group of FAPs. The MUAVE simulator allows considering multiple GUs groups and their data rate requirements for computing the energy consumption for multiple FAPs providing wireless connectivity to the groups of GUs. In what follows, we refer to the input parameters considered by the simulator, its implementation, and the output MUAVE provides.

4.1 Simulator Input Parameters

The MUAVE simulator considers a set of input parameters needed to calculate the multi-UAV energy consumption. The FSPL model is used to calculate SNR values for the links, in order to obtain the intersection areas. For the wireless links, we considered the IEEE 802.11ac technology. All the network parameters (channel bandwidth, guard interval, carrier frequency, transmission power) are configurable. The values used in our configuration are presented in Table 4.1. The transmission power is assumed to be the same for all the nodes. The final configuration established is the relationship between the required SNR for each MCS index. The maximum achievable data rate is influenced by the number of GUs sharing the channel. For that purpose, the fair share for each GU is assumed to be equal to the data rate of each MCS index divided by the number of GUs. The minimum SNR threshold for each MCS index as well as the achievable data rates are presented in Table 4.2. In order to determine the expected data rate, we set up an ns-3 simulation with 2 nodes. We progressively increased the distances between the 2 nodes and registered the

Table 4.1: Network parameters.

Notation	Physical definition	Value
B	Bandwidth	160 MHz
GI	Guard interval	800 ns
WC	Wireless channel	50
f	Channel frequency	5250 MHz
P_t	Transmission power	20 dBm

maximum distance allowed for the selection of each MCS index by the *IdealWifiManager* mechanism, associated with a given data rate. From those distances, we calculated the SNR values achieved for the wireless link established, using the FSPL model.

Regarding UAV energy consumption, several parameters that allow characterizing the UAV model and environment characteristics are worth considering. We considered the parameters presented in [2]. Additionally, since we employ an extended version of the energy model proposed in [2], we also considered the gravitational acceleration. These parameters are presented in Table 4.3.

Table 4.3: UAV and environment parameters.

Notation	Physical definition	Value
W	UAV weight	20 N
R	Rotor radius	0.4 m
Ω	Blade angular velocity	300 rad/s
k	Incremental correction factor to induced power	0.1
δ	Profile drag coefficient	0.012
ρ	Air density	1.225 kg/m
g	Gravitational acceleration	9.8 m/s^2
A	Rotor disc area ($A = \pi R^2$)	0.503 m
U_{tip}	Tip speed of the rotor blade U_{tip}	120 m/s
d_0	Fuselage drag ratio	0.6
v_0	Mean rotor induced velocity in hovering state ($v_0 = \sqrt{\frac{W}{2\rho A}}$)	4.03
s	Rotor solidity	0.05
P_b	Blade profile power in hovering state ($P_b = \frac{\delta}{8}\rho s A \Omega^3 R^3$)	79.86
P_{ind}	Induced power in hovering state ($P_{ind} = (1+k)\frac{W^{3/2}}{\sqrt{2\rho A}}$)	88.63

Table 4.2: Relation between minimum targeted SNR and expected Data Rate for a number of ground users equal to N, considering the IEEE 802.11ac technology and 160 MHz channel bandwidth.

SNR (dB)	**Data Rate (Mbit/s)**
13.1	$53/N$
13.6	$103/N$
16.1	$152/N$
19.5	$198/N$
22.6	$287/N$
27.1	$368/N$
28.4	$405/N$
29.9	$447/N$
34.1	$518/N$
35.3	$553/N$

4.2 Simulator Implementation

Considering as input the groups of GUs, including the position of each GUs and their data rate requirements, MUAVE simulator calculates the intersection area for each group of GUs. In our case, considering a given altitude provided as input, we focus exclusively on the intersection area at that particular altitude, disregarding the rest of the intersection volume. This results in an area consisting of points at a predefined distance step from each other, as depicted in Fig. 4.1. In our configuration, we considered a step of 1 meter. Similarly to UAV Power Simulator, the MUAVE simulator utilizes the Matplotlib [23] package to generate a graphical representation.

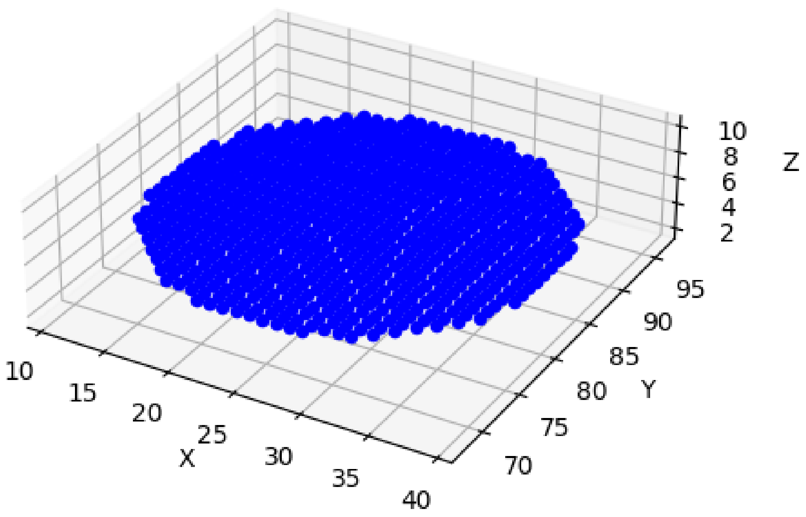

Figure 4.1: Illustrative intersection area.

In order to check for potential collisions, MUAVE first calculates the points of intersection and then stores these points for each intersection area. Then, the simulator compares the points in the newly calculated area with all the points stored from the previous calculated areas. If any compared points are the same, they are removed from the new intersection area. Then it calculates the centroid of the intersection areas following the same approach, used in the UAV Power Simulator. Since the area is made of individual points that make up the perimeter it is necessary to select the points that form the outermost boundary of the area. For that purpose, it calculates the the perimeter of the area by choosing, for each valid value of the x coordinate, the points with minimum and maximum values of the y coordinate. It also adds all the points with minimum and maximum values of the x coordinate. The centroid and perimeter are fundamental to define the three types of SUPPLY trajectories, as explained in Chapter 3.

To conduct the necessary calculation using the power consumption model given by Eq. (3.3), the function P was created. Taking as arguments the UAV flying speed V and the radius of the curve r associated with a given trajectory by the UAV, the function P allows computing the value of power consumption.

```
def P(V,r):
    firstElement= P0*(1+(3*math.pow(V,2)/(math.pow(Utip,2))))
    square=1+math.pow(math.pow(V,2)/r,2)/math.pow(g,2)
        +(math.pow(V,4)/(4*math.pow(V0,4)))
    secondElement=Pi*math.sqrt(1+math.pow(math.pow(V,2)/r,2)/math.pow(g,2))
        *math.pow((math.sqrt(square)
        -(math.pow(V,2)/(2*math.pow(V0,2)))),1/2)
    thirdElement=(1/2)*d0*rho*s*A*math.pow(V,3)
    return firstElement+secondElement+thirdElement
```

The first, second and third elements in P represent the blade profile, the induced and the parasite components in Eq. (3.3), respectively. The radius is predefined by the trajectory line. To determine the ideal flying speed V to be given as argument to P, it is necessary to calculate the value that minimizes the resulting power consumption value. In order to achieve this, we also use the optimization method from the SciPy [24] package.

With the power model implemented, MUAVE is able to determine energy consumption results for the SUPPLY trajectories. For the case of the Circular trajectory, a single flying speed value and resulting power consumption is calculated. Regarding the Oval Circular and Oval Area trajectories, they consist of 2 straight lines segments and 2 semi-circles. Therefore, to achieve the lowest power consumption possible, we optimize the flying speed value for the distinct trajectory segments. This results in different flying speeds and power consumptions optimized for the straight line movement and for the circular movement that compose these trajectories. After that, knowing the length and the optimal flying speeds for each trajectory's segment, MUAVE calculates the time during which the FAP is in a circular movement and in a straight line movement. With this information it determines the average power consumption for the entire trajectory. For the particular scenario where the FAP is placed in hovering state, the power consumption is determined by setting the flying speed to 0 m/s, while r approaches infinity. Since we may be dealing with multi-FAP scenarios, to compare trajectories, it calculates the energy consumption during a FAP flight time of 1 hour for all the trajectories. Then, the SUPPLY algorithm chooses the trajectory to be employed by the FAP.

Additionally, MUAVE also defines and calculates the energy consumption associated with the EREP algorithm trajectories, a state of the art algorithm proposed in [16]. This allows to compare the energy consumption of the trajectories defined by the SUPPLY algorithm with the ones defined by EREP. The EREP trajectories are made out of waypoints inside the intersection area, and the FAP should follow straight lines between each waypoint. However, they rely on an energy approximation when the UAV changes directions in the waypoints. Since the energy consumption model used did not account for the acceleration needed to make such direction changes, it was assumed that the UAV would be hovering for 1s. For this reason, they are solely employed for the purpose of comparison as they are not considered in the SUPPLY algorithm.

Lastly, and also for comparison reasons, MUAVE calculates the energy consumption per hour for the optimal state. This state would be achieved if we could keep the FAP only moving in a straight line at the optimal constant speed. This is an unrealistic scenario, due to the limited area for FAP movement.

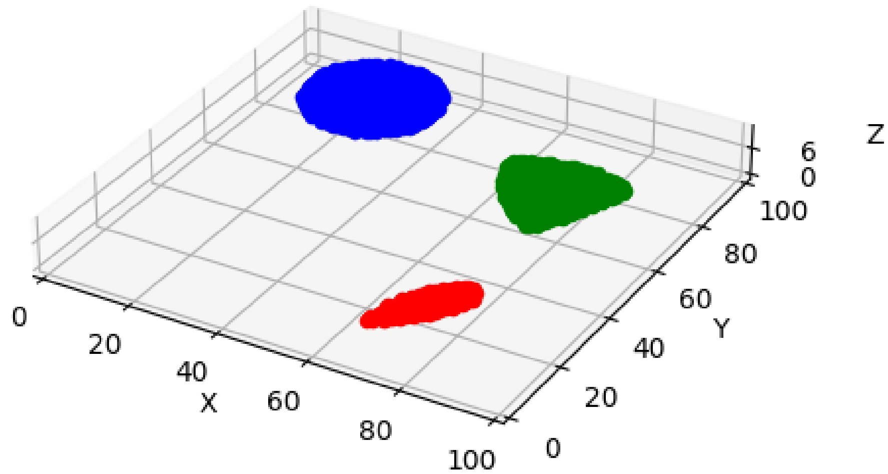

Figure 4.2: Representative output for all intersection areas defined by the MUAVE simulator in a 3D representation. Each intersection area is represented by a unique color.

4.3 Simulator Output

The MUAVE simulator provides several results as output. As an example, the output results presented in this section are obtained for a scenario consisting of 10 GUs, which led to the formation of 3 groups of GUs. First, a 3D representation of all the intersection areas is obtained, as shown in Fig. 4.2. Then, a graphical representation of the results for energy consumption per hour, which include the results for the hovering state, the optimal state, the 3 individual SUPPLY trajectories, the EREP algorithm and the SUPPLY algorithm is obtained (cf. Fig. 4.3). The colored bars represent the result for the trajectories, while the black bars represent other states of FAP movement.

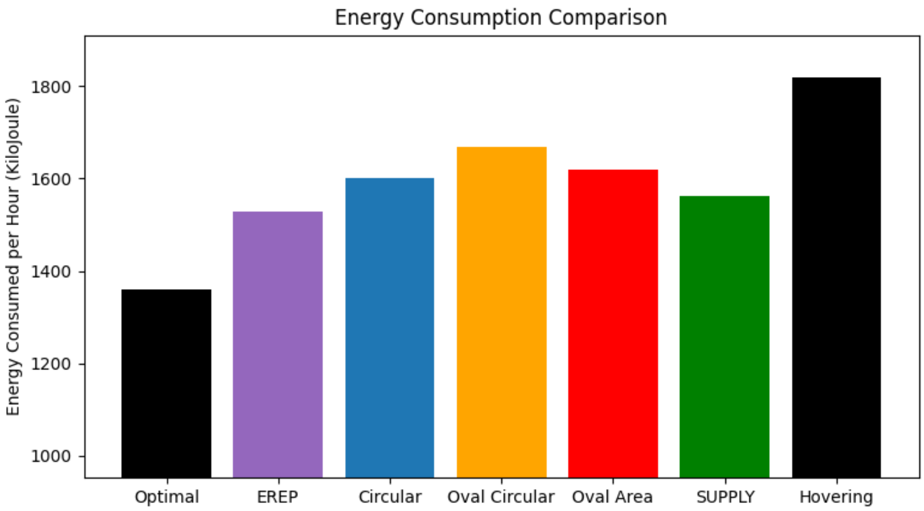

Figure 4.3: Representative output of energy consumption per hour results.

Furthermore, text files are generated, containing a detailed record of the FAPs' movement over time, position coordinates and corresponding time stamps used to describe the trajectories followed by the FAPs, as depicted in Fig. 4.4. Additionally, it outputs generic information, including intermediate results, such as calculated radiuses, powers and trajectories chosen (cf. Fig. A.1).

```
FAP: 1
30,27.15,68.24
31,31.1,69.48
32,34.52,71.83
33,37.09,75.09
34,38.59,78.95
35,38.89,83.09
36,37.95,87.13
37,35.87,90.71
38,32.82,93.53
39,29.08,95.32
40,24.98,95.93
41,20.88,95.3
42,17.14,93.5
43,14.1,90.68
44,12.03,87.08
45,11.11,83.04
46,11.42,78.91
47,12.93,75.05
48,15.51,71.8
49,18.94,69.46
50,22.9,68.23
```

Figure 4.4: Representative text file with a trajectory description. From left to right, each line indicates the target time, x coordinate, and y coordinate for each trajectory waypoint.

4.4 Summary

This chapter described the MUAVE simulator, a tool developed to compute trajectories for UAVs and calculate their energy consumption. The input parameters, including network parameters, and UAV and environment parameters, were presented and reference values were defined. Moreover, the implementation of the MUAVE simulator was described and the outputs of the MUAVE simulator were presented.

Chapter 5

SUPPLY Evaluation

In this chapter, we focus on evaluating the multi-UAV energy consumption when employing the SUPPLY algorithm and the network performance achieved when considering the three trajectories defined by SUPPLY. We begin by describing the evaluation metrics considered and the evaluation methodology used. Then, we present the results of the evaluation carried out through ns-3 simulations and discuss the obtained results. Finally, we draw the main conclusions based on the evaluation findings.

5.1 Energy Consumption and Network Performance Evaluation

To perform the energy consumption evaluation we employed the MUAVE simulator. In order to evaluate the network performance, we used the ns-3 simulator [25]. Based on the FN model presented in Chapter 3, we defined multiple scenarios with the objective of evaluating how the SUPPLY algorithm was able to define energy-efficient trajectories while assuring the targeted QoS requirements. All the considered scenarios consist of a variable number of GUs. These GUs are randomly distributed in a 100×100 meters area and have heterogeneous QoS requirements.

We considered a unique channel for each group, since the focus of this work is not the management of the wireless channel allocation. The FAPs act as independent Access Points. For traffic generation purposes, we considered a maximum channel capacity of 500 Mbit/s, which is divided by the number of GUs sharing the channel. Increasing the number of GUs sharing the channel leads to lower channel capacity available for each user. In order to ensure that the channel was not saturated, which would impact the performance results, the maximum channel capacity was reduced when increasing the number of GUs.

Depending on the networking scenario employed, the groups of GUs formed by the SUPPLY algorithm may lead to the usage of a single FAP or multiple FAPs. The FAPs are limited to the intersection's areas calculated by the SUPPLY algorithm. However, these areas may include points outside the area defined for the GUs. Allowing the areas to extend out of the defined area for the GUs has the potential to reduce energy consumption, since this may lead to larger intersection areas.

For network performance evaluation two QoS metrics were considered: 1) average throughput – average number of bits received per second by a FAP considering all GUs in the group; 2) average packet delay – the average time a packet takes to reach the sink application of each FAP, starting from the moment the packet is generated at the GU. The packet delay includes queuing, transmission, and propagation delays. Since the FAP may receive packets from multiple GUs, an average of the delay associated with those packets is calculated at each second during the simulation. In the performance evaluation carried out a special emphasis is given to throughput as it allows to prove the traffic-awareness of the proposed algorithm, considering as reference the data rate associated with the generated traffic flows. The average throughput results measured at each FAP are presented by means of a Complementary Cumulative Distribution Function (CCDF) while the average packet delay results are represented by the Cumulative Distribution Function (CDF). For channel modelling we used the FSPL model. To enhance the validation process, we also introduced a Rician fast-fading component, considering a Rician K-factor equal to 13 dB, which was derived in [26] based on experimental results.

5.1.1 ns-3 Simulation Setup

The ns-3 simulation for network performance evaluation was developed with the following configurations. For each node representing a GU a Network Interface Card (NIC) was configured in Ad Hoc mode. The IEEE 802.11ac standard was considered and the two 160 MHz available channels, 50 and 114, were used. The UDP traffic was employed, with the traffic being generated according to a Poisson distribution. Each data packet had a size of 1400 bytes. To manage the physical data rates of the wireless links, the automatic rate mechanism *IdealWifiManager* was used. The simulation duration was set to 70 seconds, with additional 30 seconds to start the applications and allow the network to reach a steady state. To manage the queues and mitigate the bufferbloat problem in the simulation, the Controlled Delay (CoDeL) algorithm [27] was employed. The simulation parameters are presented in Table 5.1.

Table 5.1: Simulation parameters.

Definition	**Value**
WiFi Standard	IEEE 802.11ac
Channel Bandwidth	160 MHz
Wireless channels	50, 114
Traffic Type	UDP
Packet Size	1400 B
Simulation time	70 s

5.1.2 Evaluation Under Typical Networking Scenarios

In this section, we present the results for typical networking scenarios. We considered 2 scenarios with 2 GUs, 2 scenarios with 5 GUs, and 2 scenarios with 10 GUs in the network. For each scenario, the positions and traffic demand of the GUs were randomly defined. For each number of GUS, one of the scenarios results in the formation of a single group (1 FAP used) and the other leads to the formation of 2 groups (2 FAPs used). Every trajectory was simulated 10 times for each scenario evaluated.

5.1.2.1 2 GUs

The first scenario considered 2 GUs positioned at $(x_1, y_1, z_1) = (47, 32, 0)$ and $(x_2, y_2, z_2) = (52, 71, 0)$, respectively. The traffic flow was randomly selected up to an aggregated value of 500 Mbit/s. They were generating 200 Mbit/s and 117.0 Mbit/s of traffic, respectively. The results for energy consumption per hour are presented in Fig. 5.1. The circular trajectory resulted in an energy consumption per hour of 474.36 kJ, the oval circular in 503.97 kJ, and the oval area in 507.81 kJ, while the hovering state resulted in 606.54 kJ. Every trajectory defined by the SUPPLY algorithm reduces energy consumption. However, in this case, the SUPPLY algorithm selected the circular trajectory, as it led to less energy consumption, with a reduction of 22% in relation to the hovering state. Regarding network performance, for the average throughput, the results show that for the SUPPLY trajectories there was no significant impact in relation to the hovering state ($< 0.5\%$), assuring the expected average 158.5 Mbit/s, as depicted in Fig. 5.2a. In terms of delay, there was a small increase when using any of the SUPPLY trajectories, but it is most noticeable in the case of the oval area where the 90^{th} percentile shows an increase of approximately 5 ms, as illustrated in 5.2b.

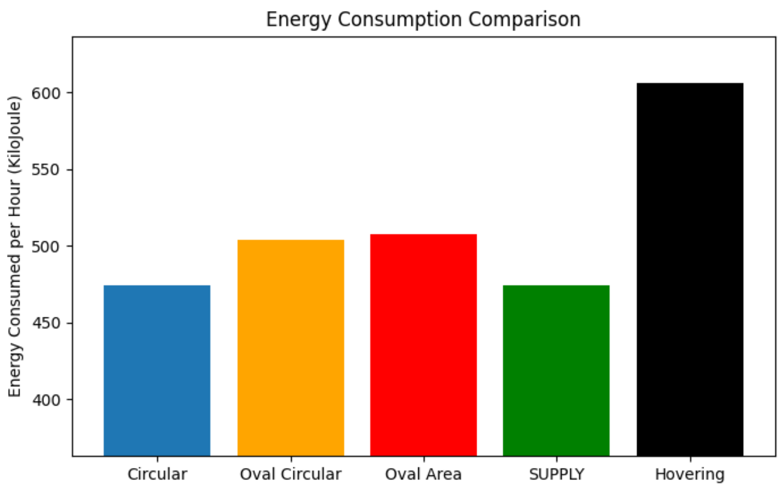

Figure 5.1: Comparison of energy consumption per hour for 2 GUs in the same group.

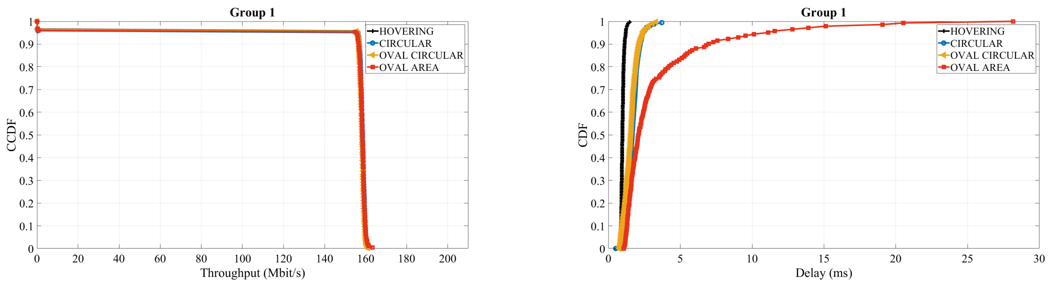

(a) Average Throughput.

(b) Delay.

Figure 5.2: Network performance results for 2 GUS in the same group.

Introducing the Rician fast-fading in addition to the FSPL model, led to a decrease in average throughput for the Oval Area and Circular trajectory. The same trajectories also resulted in increased delay, as shown in Fig. 5.3.

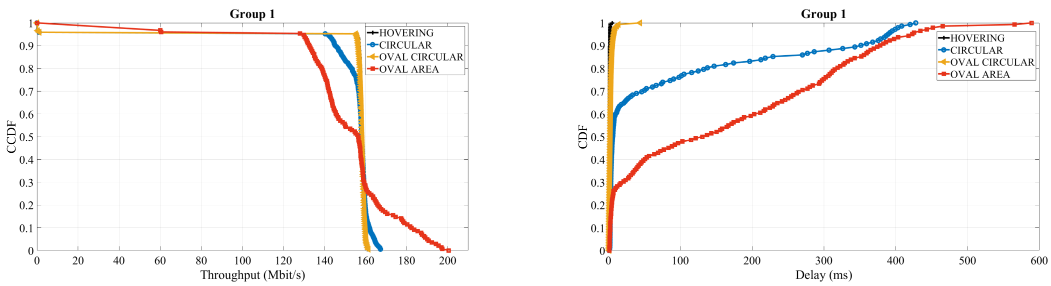

(a) Average Throughput.

(b) Delay.

Figure 5.3: Network performance results, considering the Rician fast-fading component, for 2 GUS in the same group.

By considering an SNR margin of 1 dB in the SUPPLY algorithm, we were able to obtain results close to those obtained with the FAP in the hovering state, as depicted in Fig. 5.4. The SNR margin leads to smaller intersection areas, restricting the FAPs to follow trajectories that are closer to the GUs. This also affects energy consumption, lowering to 20% the reduction in relation to the hovering state (cf. Fig. A.2).

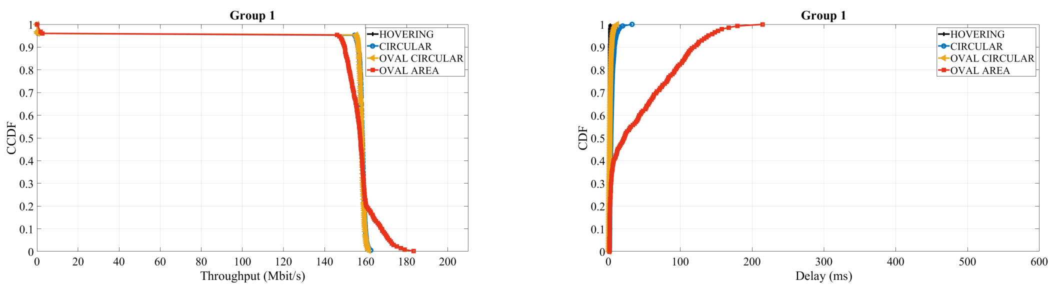

(a) Average Throughput.

(b) Delay.

Figure 5.4: Network performance results, considering the Rician fast-fading component and SNR margin of 1 dB, for 2 GUS in the same group.

The second scenario considered 2 GUs positioned at $(x_1, y_1, z_1) = (27, 17, 0)$ and the other at $(x_2, y_2, z_2) = (91, 60, 0)$. They were generating 174 Mbit/s and 208 Mbit/s of traffic, respectively. This scenario implied the usage of 2 FAPs, each serving one of the GUs. Choosing the same type of trajectory for the FAPs conducted to the following results: circular trajectory with an energy consumption per hour of 936.99 kJ, oval circular with 986.67 kJ, oval area with 1014.54 kJ, while the hovering state with 1213.09 kJ, as depicted in Fig. 5.5. As such, the SUPPLY algorithm chose the circular trajectory for both FAPs, with a reduction in energy consumption of 23% when compared with the hovering state. Regarding network performance, for the average throughput, the trajectories selected by SUPPLY do not affect the results achieved in relation to the hovering state, as illustrated in Fig. 5.6a and Fig. 5.6c. In terms of delay, the percentiles indicate an increase for Group 1 and a decrease for Group 2. However, the difference is negligible, since the values are below 1 ms for all the trajectories, as depicted in Fig. 5.6b and Fig. 5.6d.

When adding the Rician fast-fading component, no significant differences were observed (cf. A.5). As such, no SNR margin was considered.

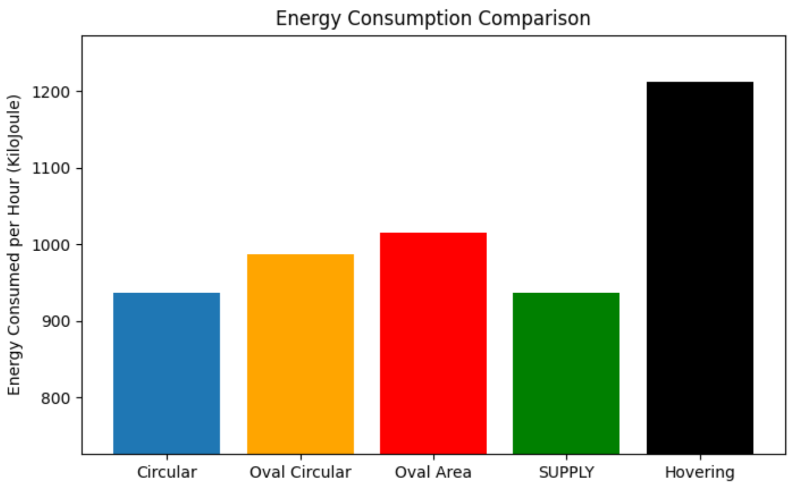

Figure 5.5: Comparison of energy consumption per hour for 2 GUs in 2 separate groups.

5.1.2.2 5 GUs

The first scenario considered 5 GUs positioned at $(x_1, y_1, z_1) = (19, 62, 0)$, $(x_2, y_2, z_2) = (85, 46, 0)$, $(x_3, y_3, z_3) = (86, 53, 0)$, $(x_4, y_4, z_4) = (2, 9, 0)$, and $(x_5, y_5, z_5) = (52, 88, 0)$, generating 36 Mbit/s, 27 Mbit/s, 19 Mbit/s, 14 Mbit/s, and 23 Mbit/s, respectively. These values were randomly defined, considering a maximum channel capacity of 250 Mbit/s, since 5 GUs were sharing the same channel. The results for energy consumption per hour are presented in Fig. 5.7. The circular trajectory resulted in an energy consumption per hour of 456.43 kJ, the oval circular in 464.46 kJ, and the oval area in 478.13 kJ, while the hovering state resulted in 606.54 kJ. The SUPPLY algorithm chose the Circular trajectory, with an energy consumption reduction of 25% in relation

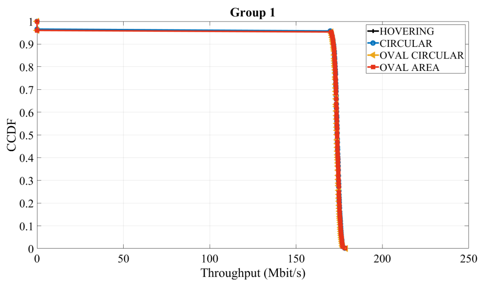

(a) Average Throughput for Group 1.

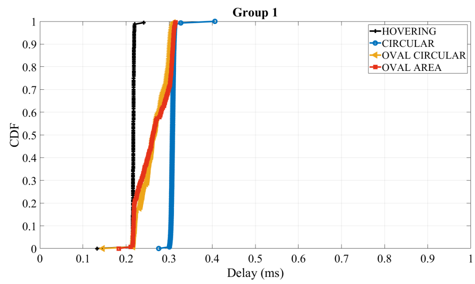

(b) Delay for Group 1.

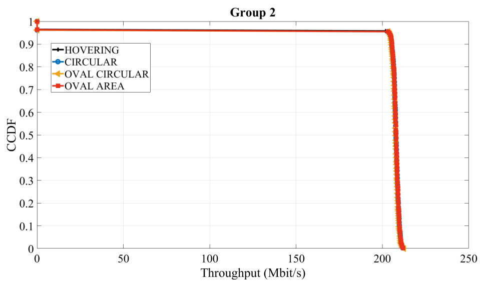

(c) Average Throughput for Group 2.

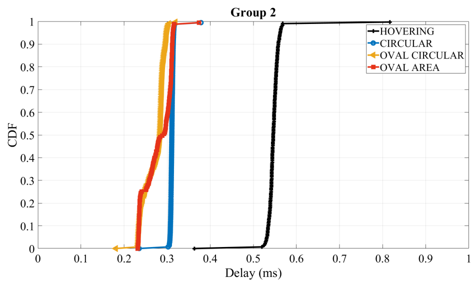

(d) Delay for Group 2.

Figure 5.6: Network performance results for 2 GUS in separate groups.

to the hovering state. In terms of network performance, the average throughput results show that for the SUPPLY trajectories there was no significant impact in relation to the hovering state ($< 0,5\%$), allowing to guarantee 23.8 Mbit/s, as depicted in Fig. 5.8a. When it comes to delay, there was an increase when using the SUPPLY trajectories up to at most 20 ms, for the 90^{th} percentile, as illustrated in Fig. 5.8b.

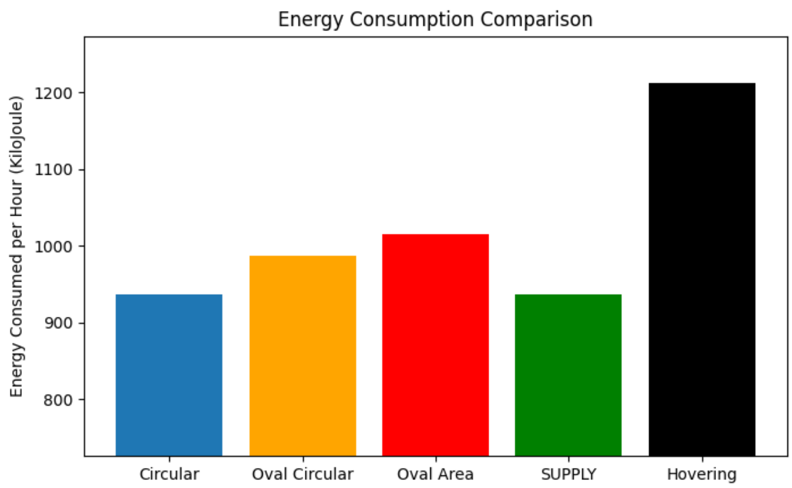

Figure 5.7: Comparison of energy consumption per hour for 5 GUs in the same group.

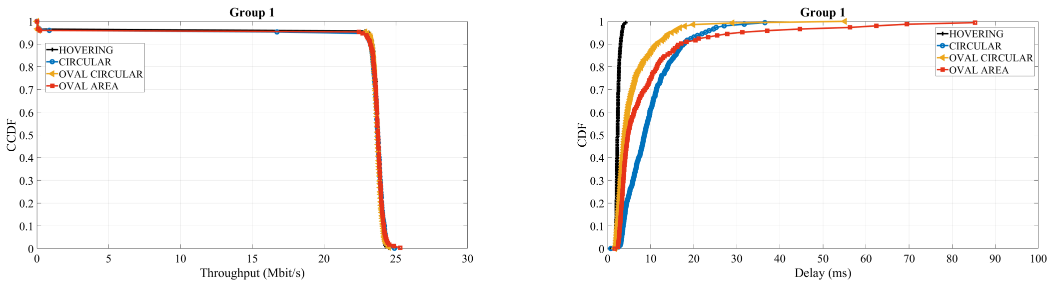

(a) Average Throughput. (b) Delay.

Figure 5.8: Network performance results for 5 GUS in the same group.

When considering the Rician fast-fading in addition to the FSPL model, the network performance results show the average throughput, for the oval area and circular trajectory is reduced up to 50%, as shown in Fig. 5.9a. An increase in the average packet delay was also observed in Fig. 5.9b.

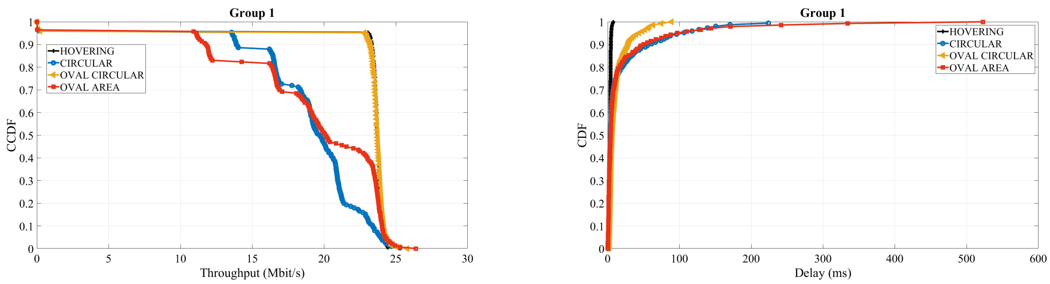

(a) Average Throughput. (b) Delay.

Figure 5.9: Network performance results, considering the Rician fast-fading component, for 5 GUS in the same group.

By considering SNR margin of 1 dB in the SUPPLY algorithm, we were able to obtain results close to those obtained with the FAP in a hovering state; only the oval area trajectory was not able to assure QoS during the whole simulation time, as seen in Fig. 5.10a. The delay results were also improved when compared to the case where no SNR margin is employed, as depicted in Fig. 5.10b. The introduction of the SNR margin also did not affect the energy consumption (cf. Fig. A.3).

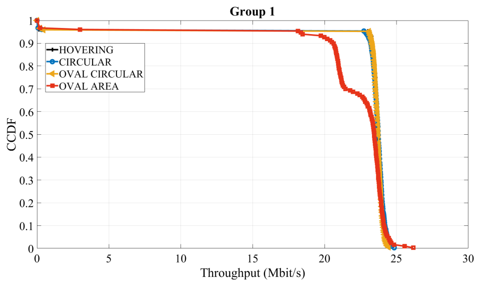

(a) Average Throughput.

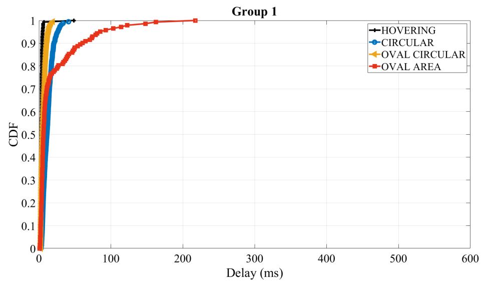

(b) Delay.

Figure 5.10: Network performance results, considering the Rician fast-fading model and SNR margin of 1 dB, for 5 GUS in the same group.

The second scenario considered 5 GUs positioned at $(x_1, y_1, z_1) = (58, 56, 0)$, $(x_2, y_2, z_2) = (24, 88, 0)$, $(x_3, y_3, z_3) = (35, 92, 0)$, $(x_4, y_4, z_4) = (60, 25, 0)$, and $(x_5, y_5, z_5) = (51, 14, 0)$, generating 73 Mbit/s, 42 Mbit/s, 87 Mbit/s, 11 Mbit/s, and 71 Mbit/s of traffic, respectively. These traffic demand values were randomly selected, considering a maximum channel capacity of 500 Mbit/s. The SUPPLY algorithm imposed the creation of 2 groups served by 2 FAPs. FAP_1 was serving the group composed of GU_1, GU_2, and GU_3 while FAP_2 was serving the group composed of GU_4 and GU_5. Choosing the same type of trajectory for the FAPs would lead to the following results: circular trajectory with an energy consumption per hour of 998.00 kJ, oval circular with 1044.60 kJ and oval area with 1022.51 kJ, while the hovering state would result in 1213.09 kJ, as seen in Fig. 5.11. In order to optimize energy consumption, the SUPPLY algorithm chose different trajectories for each FAP. For FAP_1, SUPPLY selected the oval area trajectory and for FAP_2 the circular trajectory. This resulted in an energy consumption per hour of 986.75 kJ, which is 19% less when compared with the hovering state. Regarding network performance, the average throughput results show that the SUPPLY trajectories do not introduce a significant impact in relation to the hovering state, assuring the 67.3 Mbit/s and 41 Mbit/s, as illustrated in Fig. 5.12a and Fig. 5.12c. No significant delay increases were also noted, as demonstrated in Fig. 5.12b and Fig. 5.12d.

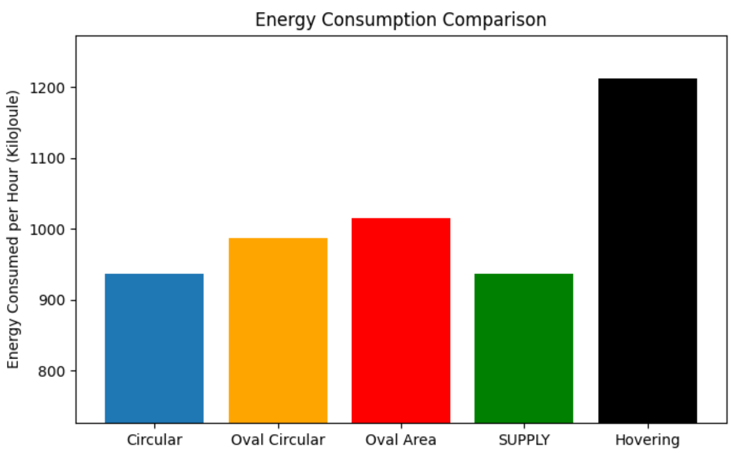

Figure 5.11: Comparison of energy consumption per hour for 5 GUs in 2 separate groups.

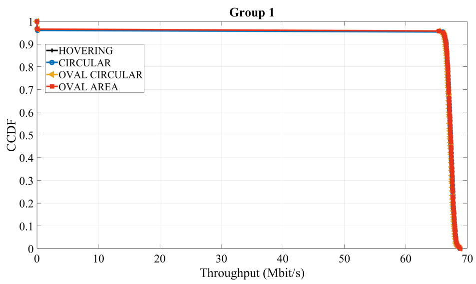

(a) Average Throughput for Group 1.

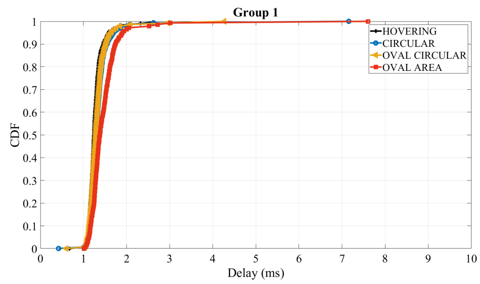

(b) Delay for Group 1.

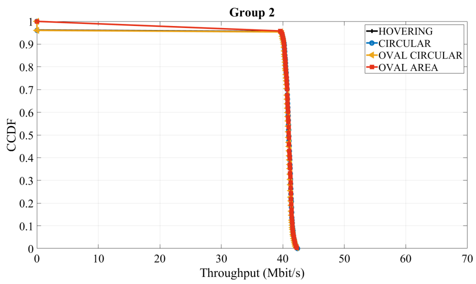

(c) Average Throughput for Group 2.

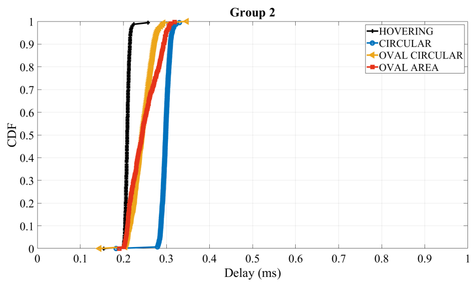

(d) Delay for Group 2.

Figure 5.12: Network performance results for 5 GUS in 2 separate groups.

When considering the Rician fast-fading component, similar results were achieved (cf. Fig. A.6). As such, no SNR margin was required.

5.1.2.3 10 GUs

The first scenario considered 10 GUs positioned at $(x_1,y_1,z_1) = (69,83,0)$, $(x_2,y_2,z_2) = (68,91,0)$, $(x_3,y_3,z_3) = (26,16,0)$, $(x_4,y_4,z_4) = (67,8,0)$, $(x_5,y_5,z_5) = (38,21,0)$, $(x_6,y_6,z_6) = (23,71,0)$, $(x_7,y_7,z_7) = (60,34,0)$, $(x_8,y_8,z_8) = (8,31,0)$, $(x_9,y_9,z_9) = (59,59,0)$, and $(x_{10},y_{10},z_{10}) = (20,79,0)$. They were generating 9 Mbit/s, 6 Mbit/s, 1 Mbit/s, 5 Mbit/s, 3 Mbit/s, 6 Mbit/s, 7 Mbit/s, 5 Mbit/s, 8 Mbit/s, and 6 Mbit/s, respectively. The traffic demand values were randomly defined, considering a maximum aggregated value of 100 Mbit/s since 10 GUs were sharing the same channel. The results for energy consumption per hour are presented in Fig. 5.13. The circular trajectory resulted in an energy consumption per hour of 454.45 kJ, the oval circular in 457.18 kJ and the oval area in 469.22 kJ, while the hovering state resulted in 606.54 kJ. The SUPPLY algorithm chose the circular trajectory, with an energy consumption reduction of 25% in relation to the hovering state. In terms of network performance, the results show that the difference in average throughput between the SUPPLY trajectories and the hovering state is negligible, both allowing for 5.6 Mbit/s, as can be seen in Fig. 5.8a. For delay, there was an increase when using the SUPPLY trajectories, most noticeable in the circular trajectory. The results show an increase in the range of 5 to 15 ms for this trajectory, as depicted in Fig. 5.8b.

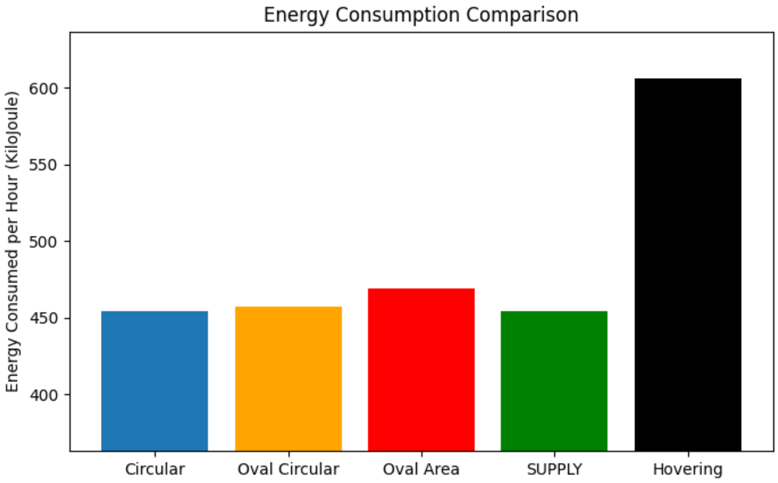

Figure 5.13: Comparison of energy consumption per hour for 10 GUs in the same group.

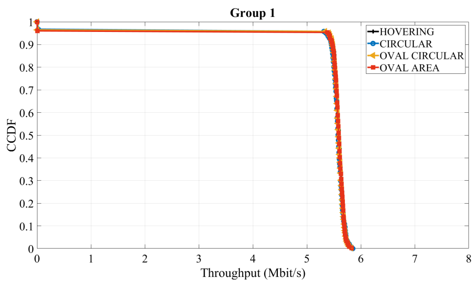

(a) Average Throughput.

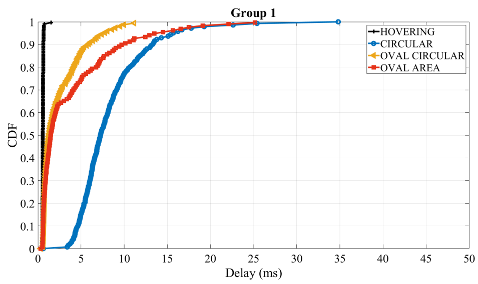

(b) Delay.

Figure 5.14: Network performance results for 10 GUS in the same group.

Introducing the Rician fast-fading in addition to the FSPL model, led to a decrease in average throughput for the SUPPLY trajectories. This is most noticeable for the circular and oval area trajectories. The 90^{th} percentiles in Fig. 5.15a show a decrease of 21% and 28% of the expected throughput. The results also denote increased delay, as depicted in Fig. 5.15b.

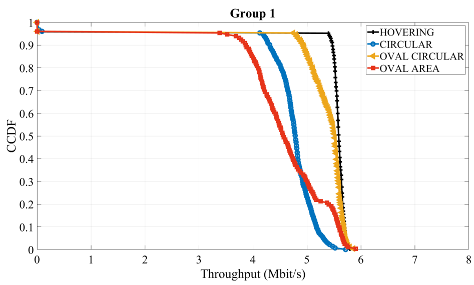

(a) Average Throughput.

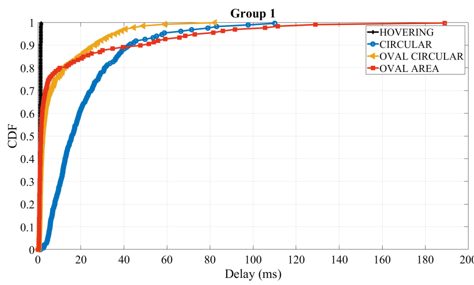

(b) Delay.

Figure 5.15: Network performance results, considering the Rician fast-fading component, for 10 GUs in the same group.

Similarly to the cases with 2 and 5 GUs, by adding a 1 dB SNR margin we were able to obtain results close to those obtained with the FAP in a hovering state. The circular and oval area trajectories imply a small decrease in the average throughput, as depicted in 5.16a. The delay results were also better when compared to the previous simulation, as shown in Fig. 5.16b. The introduction of the SNR margin did not affect energy consumption (cf. Fig. A.4).

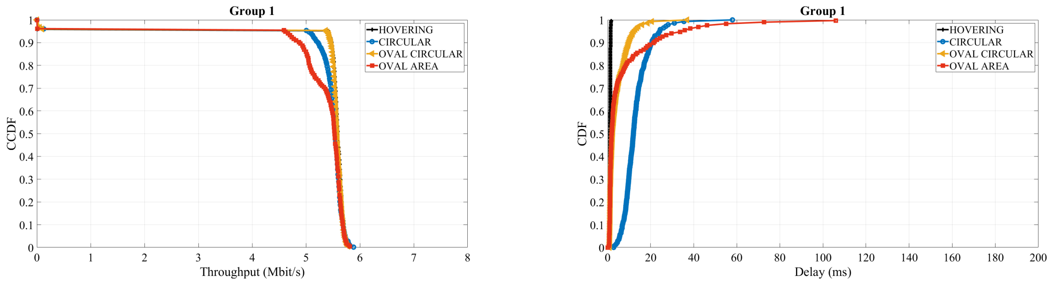

(a) Average Throughput. (b) Delay.

Figure 5.16: Network performance results, considering the Rician fast-fading component and SNR margin of 1 dB, for 10 GUS in the same group.

Finally, we considered a scenario with 10 GUs positioned at $(x_1, y_1, z_1) = (47, 27, 0)$, $(x_2, y_2, z_2) = (29, 55, 0)$, $(x_3, y_3, z_3) = (42, 30, 0)$, $(x_4, y_4, z_4) = (2, 17, 0)$, $(x_5, y_5, z_5) = (19, 49, 0)$, $(x_6, y_6, z_6) = (68, 66, 0)$, $(x_7, y_7, z_7) = (39, 15, 0)$, $(x_8, y_8, z_8) = (79, 76, 0)$, $(x_9, y_9, z_9) = (84, 7, 0)$, and $(x_{10}, y_{10}, z_{10}) = (82, 9, 0)$. They were offering 38 Mbit/s, 32 Mbit/s, 29 Mbit/s, 39 Mbit/s, 43 Mbit/s, 21 Mbit/s, 8 Mbit/s, 49 Mbit/s, 6 Mbit/s, and 14 Mbit/s, respectively; these values were randomly generated. The SUPPLY algorithm led to the creation of 2 groups served by 2 FAPs. FAP_1 was serving the group composed of GU_1, GU_2, GU_3, GU_4, GU_5, and GU_6 and FAP_2 was serving the group composed of GU_7, GU_8, GU_9, and GU_{10}. Choosing the same type of trajectory for the FAPs would lead to the following results: circular trajectory with an energy consumption per hour of 1080.35 kJ, the oval circular with 1116.75 kJ and the oval area with 1093.01 kJ, while the hovering state would result in 1213.09 kJ, as can be seen in Fig. 5.17. In this scenario the SUPPLY algorithm selected different trajectories for each FAP: FAP_1 followed the oval area trajectory, and FAP_2 followed the circular trajectory. As a result, the energy consumption per hour was 1054.41 kJ, which represents a 13% decrease with respect to the hovering state. Regarding network performance, the SUPPLY trajectories did not have a significant impact on the average throughput compared to the hovering state, assuring the expected averages of 33.7 Mbit/s and 19.3 Mbit/s, as shown in Fig. 5.18a and Fig. 5.18c. No significant delay increases were noted (cf. Fig. 5.18b and Fig. 5.18d).

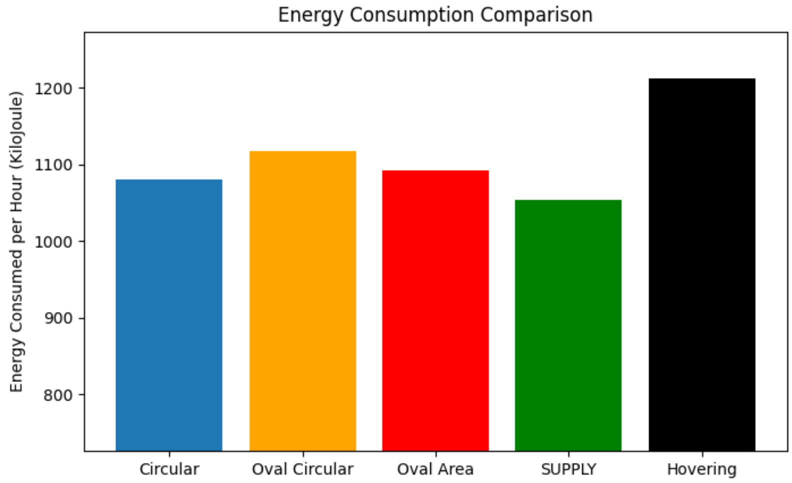

Figure 5.17: Comparison of energy consumption per hour for 10 GUs in 2 separate groups.

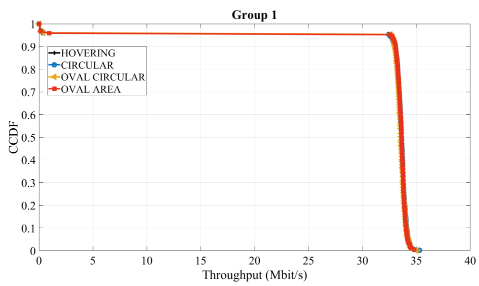

(a) Average Throughput for Group 1.

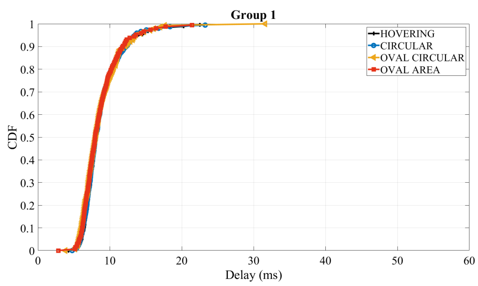

(b) Delay for Group 1.

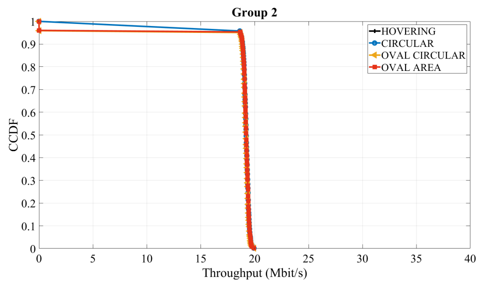

(c) Average Throughput for Group 2.

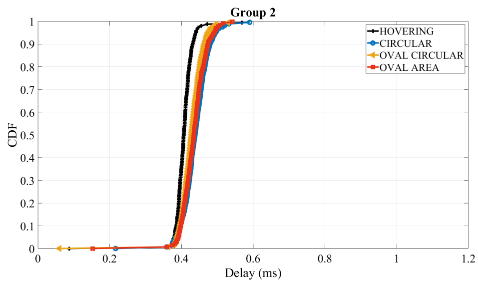

(d) Delay for Group 2.

Figure 5.18: Network performance results for 10 GUS in 2 separate groups.

When adding the Rician fast-fading component, the same results were achieved (cf. Fig. A.7). As such, no SNR margin was required.

5.1.3 Energy Evaluation for Random Networking Scenarios

Since we are capable of generating random networking scenarios by considering as input a given a number of GUs and a predefined interval to define the traffic demand for the GUs, we were able to evaluate how the number of GUs in the network influences the energy consumption results. This allowed assessing the gains achieved by the SUPPLY algorithm for generic networking scenarios. For that purpose, we generated 200 random networking scenarios for each distinct number of GUs in the network: 2, 5, and 10 GUs. The traffic flow values were randomly selected, considering a maximum channel capacity of 500 Mbit/s for all the scenarios. We then calculated the energy ratio in relation to the hovering state. The energy ratio metric is calculated dividing the SUPPLY energy consumption by the hovering state energy consumption. It can be converted to a energy reduction percentage doing $(1 - energy\_ratio) \times 100$. The results are shown in Fig. 5.19. The 50^{th} percentile reveals energy ratios of 0.76, 0.82 and 0,84 for scenarios with 2, 5, and 10 GUs, respectively. On the other hand, the 90^{th} percentile indicates energy ratios of 0.83, 0.89 and 0.91, respectively.

The obtained results allow to conclude that as the number of GUs increases, the energy gains relative to the hovering state decrease. It is also possible to note that an increase in the average number of FAPs needed with the increase in number of GUs. For scenarios with 2, 5, and 10 GUs, the average number of FAPs was 1, 2, and 3, respectively.

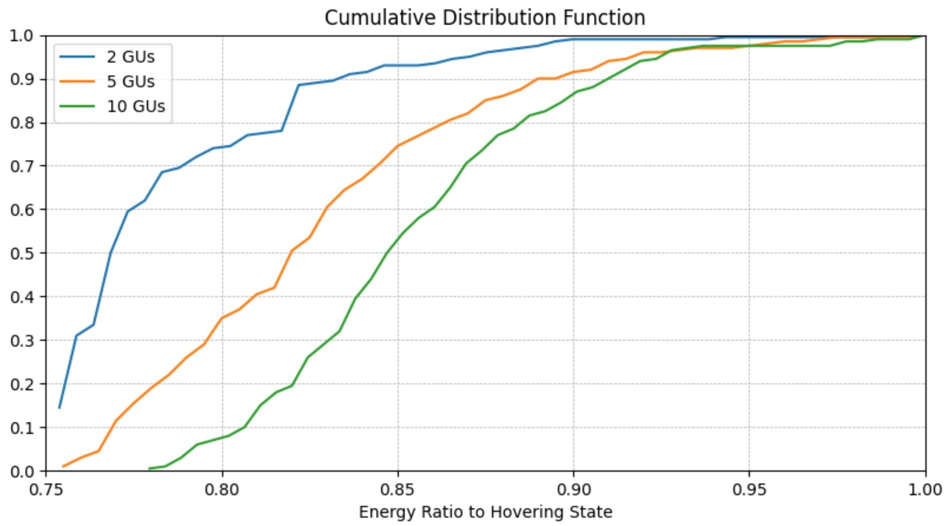

Figure 5.19: Energy ratios for the SUPPLY algorithm in relation to the hovering state considering 200 random networking scenarios for each distinct number of GUs – 2, 5, and 10.

5.2 Discussion

Overall, from the results presented in this chapter it is possible to conclude that the SUPPLY algorithm results in reduced energy consumption with minimal impact on network performance. However, some considerations were noted.

Regarding the energy consumption results, increasing the number of GUs in the area leads to less energy gains when compared to the hovering state. Due to the increased number of GUs in the same area, the SUPPLY algorithm is more likely to generate larger groups that will result in smaller intersection areas. With a smaller area to place the FAP, the SUPPLY algorithm defines less energy-efficient trajectories (with smaller straight line segments and radiuses).

The intersection of the GUs spheres may result in different shapes of intersection areas depending on the number of GUs in the group and their data rate requirements. As such, different trajectories are preferable in different shapes of intersection areas. It is observable, that for more circular shaped areas the circular trajectory is the preferable trajectory. While, for more elongated areas, the oval area trajectory leads to less energy consumption.

Regarding network performance, the SUPPLY trajectories indicate similar performance to the hovering state when considering only the FSPL model. The introduction of Rician fast-fading component, in the scenarios where all the GUs share the same channel, results in losses in performance, especially for the circular and oval area trajectories. These losses are expected since the Rician fast-fading component adds a random component to emulate performance degrading elements observed in real wireless channels. The circular and oval area trajectories are the most affected since they always reach the perimeter of the intersection area. However, by considering SNR margin of 1 dB these losses are mitigated, reaching similar performance results obtained for the scenarios without the Rician fast-fading component. Moreover, in the scenarios where drops in performance are noted for the other SUPPLY trajectories, the oval circular trajectory is able to maintain similar performance achieved by keeping the FAP in hovering. The oval circular trajectory introduces a margin by not reaching the perimeter of the intersection areas, for most cases, which explains these results. This has a similar effect to the addition of an SNR margin. However, since it does not take full advantage of the intersection area, the energy consumption results tend to be worse than the ones achieved by the other SUPPLY trajectories. For that reason, it is the least chosen trajectory by the SUPPLY algorithm.

Chapter 6

Conclusions and Future Work

UAVs have become increasingly popular in recent years due to their versatility. As UAVs are capable of hovering over the ground and carrying on-board cargo, they are suitable platforms for transporting communications nodes. In temporary events, such as emergency scenarios and crowded events, UAVs are an emerging solution to form Flying Networks (FNs) able to establish and reinforce wireless coverage and capacity on-demand.

When compared with terrestrial networks, FNs impose additional challenges. Since UAVs are not permanently connected to the electrical grid, they rely on on-board power sources, such as electric batteries, for both communications and movement. The energy consumption problem of UAVs should be considered for defining their optimal placement. In the literature, this problem has been studied and it was possible to conclude that: 1) UAV energy consumption is mainly affected by flying speed, altitude, and payload weight; 2) UAVs are more energy efficient while moving at an optimal speed rather than in hovering state; 3) Increasing the UAV altitude and payload weight increases energy consumption.

The placement of UAVs in an FN has also been the subject of study by the scientific community. For the purpose of single UAV placement recent solutions have been proposed to minimize the UAV energy consumption. For the case of multi-UAV placement, most of the state of the art solutions are focused on maximizing the coverage area. They do not consider that the Gound Users (GUs) are not homogeneously distributed and may have heterogeneous QoS requirements. In the literature, there are no solutions for multi-UAV placement that address the energy-efficient movement and allow meeting heterogeneous QoS requirements.

In order to address the problem, in this dissertation an energy and performance aware placement algorithm for multiple UAVs, named SUPPLY, was proposed. The SUPPLY takes into consideration the UAVs energy consumption and the data rate requirements of the GUs to define UAV trajectories that minimize the energy consumption while ensuring the targeted QoS requirements. Additionally, a simulation tool, named MUAVE, was developed to compute the energy consumption for multiple UAVs providing wireless connectivity to groups of GUs.

The SUPPLY algorithm was evaluated for energy consumption and network performance. For energy consumption, the evaluation relied on the MUAVE simulator. Regarding network performance the ns-3 simulator was used, centering the analysis on two metrics: average throughput and average packet delay. The obtained results led to the conclusion that employing the SUPPLY algorithm allows for reduced energy consumption with minimal network performance impact.

The work developed accomplished all the objectives. As future work, real-world experiments could be made to confirm the energy consumption values obtained using the MUAVE simulator and network performance results obtained using ns-3, and further validate the SUPPLY algorithm. In addition, other regular or irregular trajectories may be investigated and machine learning techniques, such as Reinforcement Learning, may be used to learn trajectories that lead to minimum energy consumption.

Appendix A

A.1 Additional Multi-UAV Energy Consumption Simulator Outputs

```
Minumum Power Velocity=10.212500000000011
Minimum Power=126.00271616581941
Hover Power=168.48421774108203

---Circular---
Radius:  9.307429269747411
Optimization terminated successfully.
         Current function value: 145.155622
         Iterations: 30
         Function evaluations: 60
Cirular Min Power Velocity:  6.355500000000008
Circular Power:  145.15562179801452

-----OVAL (CIRCULAR)-----
r2:  2.792228780924223
ideal:  [75.51141552511416, 66.81735159817352, 6.0]
Optimization terminated successfully.
         Current function value: 163.935993
         Iterations: 28
         Function evaluations: 56
Curve Min Power Velocity:  2.637187500000003
Curve Power:  163.93599286377673
Curve Distance: 17.544090850587047 Straight Distance: 26.060801955292753
Curve Time : 6.6525762201538665 Straight Time: 2.5518533126357625
Oval Power: 153.41930006321016

-----OVAL (AREA)-----
r2: 0.8436614877321075
Optimization terminated successfully.
         Current function value: 168.025580
         Iterations: 24
         Function evaluations: 48
Curve Min Power Velocity:  0.8272500000000009
Curve Power:  168.0255802679687
Curve Distance: 5.300881463951648 Straight Distance: 48.77897329069276
Curve Time : 6.407834951890774 Straight Time: 4.776398853433802
Oval Power: 150.07907061793324
Best: Circular
Optimal:  1360.83
Circular:  1601.64
Oval(circular):  1668.4
Oval(area):  1619.55
SUPPLY:  1563.22
EREP:  1529.26
Hovering:  1819.63
Energy Reduction (%): 14.1
```

Figure A.1: Representative terminal output of the Multi-UAV Energy Consumption Simulator.

A.2 Additional Energy Consumption Results

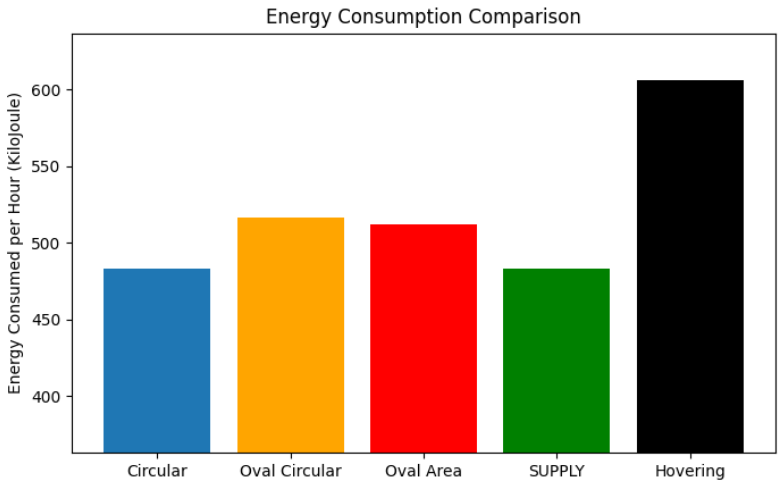

Figure A.2: Comparison of energy consumption per hour for 2 GUs in the same group with a 1 dB SNR margin.

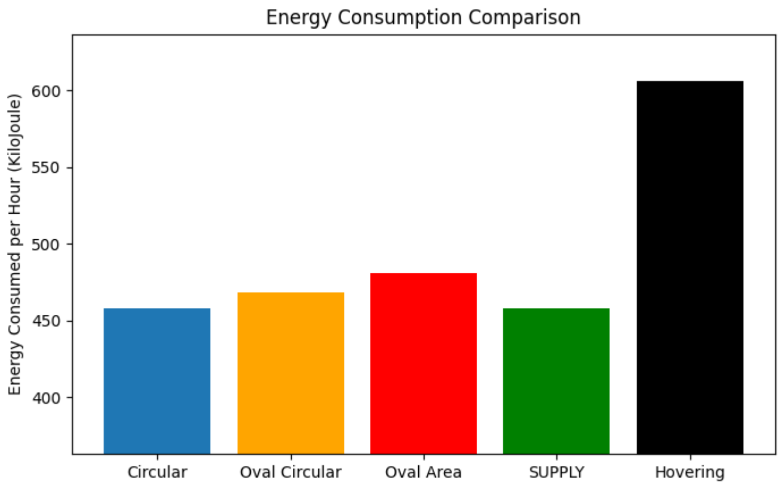

Figure A.3: Comparison of energy consumption per hour for 5 GUs in the same group with a 1 dB SNR margin.

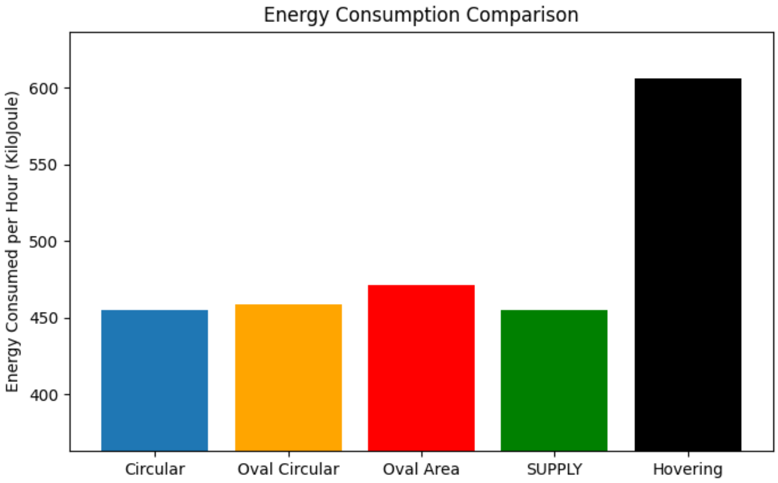

Figure A.4: Comparison of energy consumption per hour for 10 GUs in the same group with a 1 dB SNR margin.

A.3 Additional Network Performance Results

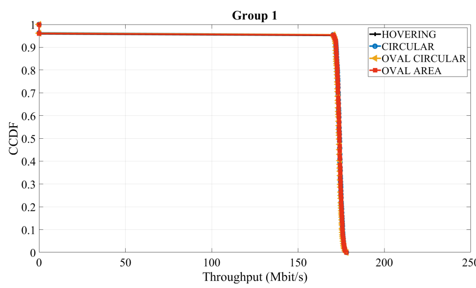

(a) Average Throughput.

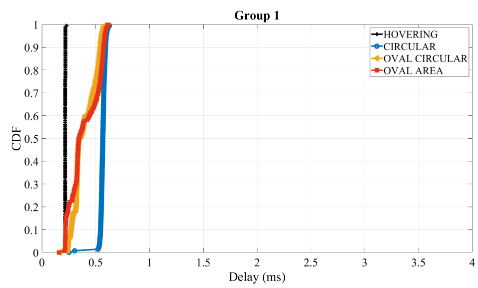

(b) Delay.

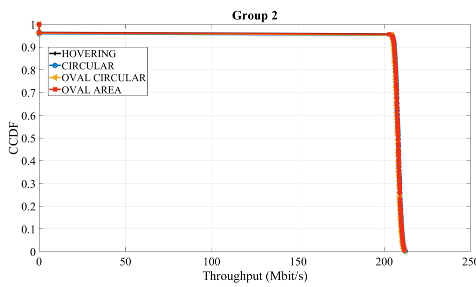

(c) Average Throughput.

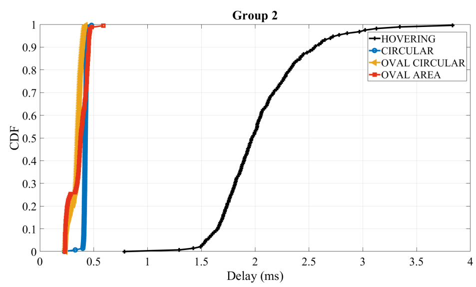

(d) Delay.

Figure A.5: Network performance results, considering the Rician fast-fading component, for 2 GUS in 2 separate groups.

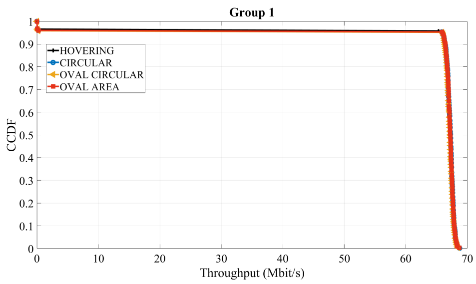

(a) Average Throughput.

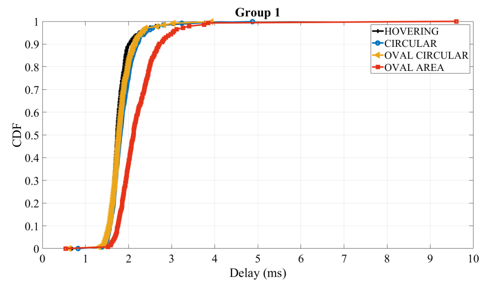

(b) Delay.

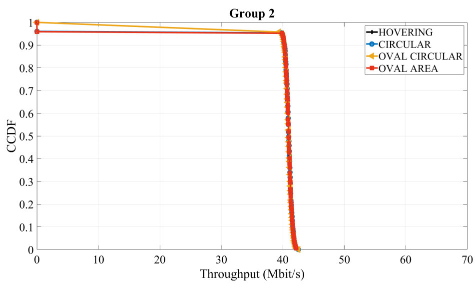

(c) Average Throughput.

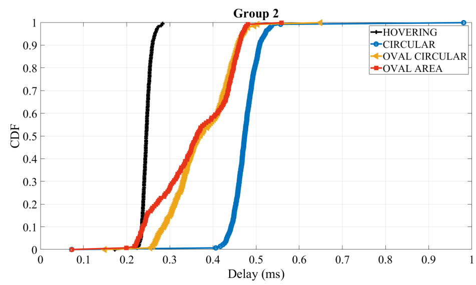

(d) Delay.

Figure A.6: Network performance results, considering the Rician fast-fading component, for 5 GUS in 2 separate groups.

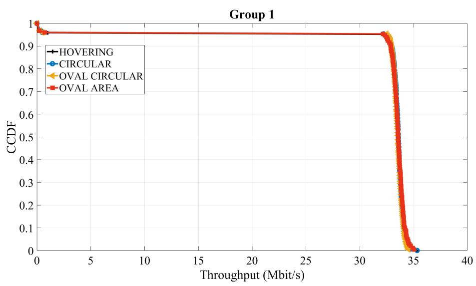

(a) Average Throughput.

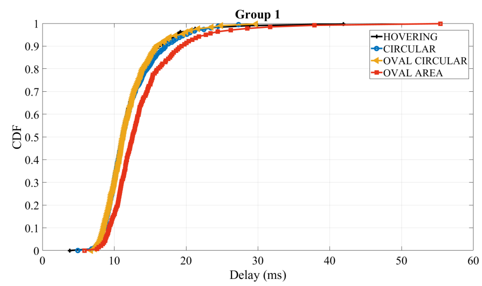

(b) Delay.

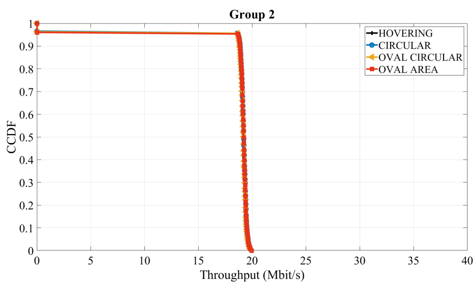

(c) Average Throughput.

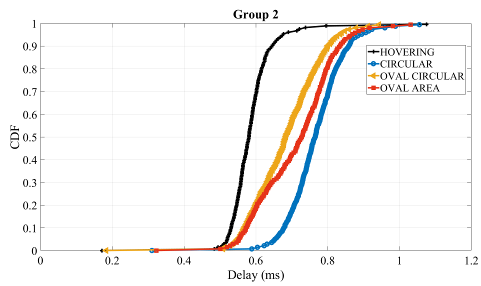

(d) Delay.

Figure A.7: Network performance results, considering the Rician fast-fading component, for 10 GUS in 2 separate groups.

References

[1] Hugo Rodrigues, André Coelho, Manuel Ricardo, and Rui Campos. Joint energy and performance aware relay positioning in flying networks. *IEEE Access*, 10:43848–43864, 2022. doi:10.1109/ACCESS.2022.3168695.

[2] Yong Zeng, Jie Xu, and Rui Zhang. Energy minimization for wireless communication with rotary-wing uav. *IEEE Transactions on Wireless Communications*, 18(4):2329–2345, 2019. doi:10.1109/TWC.2019.2902559.

[3] Uygar Demir, Merve Çiğdem İpek, Cenk Toker, and Özgür Ekici. Energy-efficient rotary-wing uav deployment under flight dynamics and qos constraints. In *2019 IEEE International Black Sea Conference on Communications and Networking (BlackSeaCom)*, pages 1–5, 2019. doi:10.1109/BlackSeaCom.2019.8812816.

[4] Carlos Muli, Sangyoung Park, and Mingming Liu. A comparative study on energy consumption models for drones, 2022. URL: https://arxiv.org/abs/2206.01609, doi:10.48550/ARXIV.2206.01609.

[5] André Coelho, Helder Fontes, Rui Campos, and Manuel Ricardo. Traffic-aware gateway placement for high-capacity flying networks. In *2021 IEEE 93rd Vehicular Technology Conference (VTC2021-Spring)*, pages 1–6, 2021. doi:10.1109/VTC2021-Spring51267.2021.9448966.

[6] Eduardo Nuno Almeida, Rui Campos, and Manuel Ricardo. Traffic-aware multi-tier flying network: Network planning for throughput improvement. In *2018 IEEE Wireless Communications and Networking Conference (WCNC)*, pages 1–6, 2018. doi:10.1109/WCNC.2018.8377408.

[7] André Coelho, Helder Fontes, Rui Campos, and Manuel Ricardo. Placement and allocation of communications resources in slicing-aware flying networks. In *2022 17th Wireless On-Demand Network Systems and Services Conference (WONS)*, pages 1–8, 2022. doi:10.23919/WONS54113.2022.9764562.

[8] Nithin Babu, Constantinos B. Papadias, and Petar Popovski. Energy-efficient 3-d deployment of aerial access points in a uav communication system. *IEEE Communications Letters*, 24(12):2883–2887, 2020. doi:10.1109/LCOMM.2020.3017559.

[9] Quang Tuan Do, Duc Thien Hua, Anh Tien Tran, and Sungrae Cho. Energy efficient multi-uav communication using ddpg. In *2022 13th International Conference on Information and Communication Technology Convergence (ICTC)*, pages 1071–1075, 2022. doi:10.1109/ICTC55196.2022.9952663.

[10] Ibrahim A. Nemer, Tarek R. Sheltami, Slim Belhaiza, and Ashraf S. Mahmoud. Energy-efficient uav movement control for fair communication coverage: A deep reinforcement learning approach. *Sensors*, 22(5), 2022. URL: https://www.mdpi.com/1424-8220/22/5/1919, doi:10.3390/s22051919.

[11] MCS table and how to use it. (Accessed: 2023-01-04). URL: https://wlanprofessionals.com/mcs-table-and-how-to-use-it/.

[12] Ning Gao, Yong Zeng, Jian Wang, Di Wu, Chaoyue Zhang, Qingheng Song, Jachen Qian, and Shi Jin. Energy model for uav communications: Experimental validation and model generalization. *China Communications*, 18(7):253–264, 2021. doi:10.23919/JCC.2021.07.020.

[13] In-flight positional and energy use data set of a dji matrice 100 quadcopter for small package delivery. *Scientific Data*, 8, 12 2021. doi:10.1038/s41597-021-00930-x.

[14] Hua Yan, Yunfei Chen, and Shuang-Hua Yang. New energy consumption model for rotary-wing uav propulsion. *IEEE Wireless Communications Letters*, 10(9):2009–2012, 2021. doi:10.1109/LWC.2021.3090772.

[15] André Coelho, Eduardo Nuno Almeida, Pedro Silva, José Ruela, Rui Campos, and Manuel Ricardo. Redefine: Centralized routing for high-capacity multi-hop flying networks. In *2018 14th International Conference on Wireless and Mobile Computing, Networking and Communications (WiMob)*, pages 75–82, 2018. doi:10.1109/WiMOB.2018.8589098.

[16] Hugo Rodrigues, André Coelho, Manuel Ricardo, and Rui Campos. Energy-aware relay positioning in flying networks. *Int. J. Commun. Syst.*, 2020. doi:10.1002/dac.5233.

[17] Hugo Rodrigues. Gateway positioning in flying networks, 7 2020. URL: https://hdl.handle.net/10216/132922.

[18] Gurobi, Jun 2023. (Accessed: 2023-6-19). URL: https://www.gurobi.com/.

[19] Minghui Dai, Ning Huang, Yuan Wu, Jie Gao, and Zhou Su. Unmanned aerial vehicles assisted wireless networks: Advancements, challenges, and solutions. *IEEE Internet of Things Journal*, pages 1–1, 2022. doi:10.1109/JIOT.2022.3230786.

[20] Andrea Goldsmith. *Wireless Communications*. Cambridge University Press, 2005. doi:10.1017/CBO9780511841224.

[21] Python. (Accessed: 2023-6-19). URL: https://www.python.org/.

[22] Hugo Rodrigues. Uav-power-simulator. (Accessed: 2023-01-04). URL: https://github.com/rhugo97/UAV-Power-Simulator.

[23] Matplotlib. (Accessed: 2023-6-22). URL: https://matplotlib.org/.

[24] Scipy. (Accessed: 2023-6-22). URL: https://www.scipy.org/.

[25] ns-3 website. (Accessed: 2023-01-04). URL: https://www.nsnam.org/.

[26] Eduardo Nuno Almeida, André Coelho, José Ruela, Rui Campos, and Manuel Ricardo. Joint traffic-aware uav placement and predictive routing for aerial networks. *Ad Hoc Networks*, 118:102525, 2021. URL: https://www.sciencedirect.com/science/article/pii/S1570870521000779, doi:https://doi.org/10.1016/j.adhoc.2021.102525.

[27] Kathleen Nichols and Van Jacobson. Controlling queue delay: A modern aqm is just one piece of the solution to bufferbloat. *Queue*, 10(5):20–34, may 2012. URL: https://doi.org/10.1145/2208917.2209336, doi:10.1145/2208917.2209336.